Advances and challenges in understanding the electrocatalytic conversion of carbon dioxide to fuels

Yuvraj Y. Birdja [1,2], Elena Pérez-Gallent[1,3], Marta C. Figueiredo [1,4], Adrien J. Göttle[1], Federico Calle-Vallejo [1,5]* and Marc T. M. Koper [1]*

The electrocatalytic reduction of carbon dioxide is a promising approach for storing (excess) renewable electricity as chemical energy in fuels. Here, we review recent advances and challenges in the understanding of electrochemical CO_2 reduction. We discuss existing models for the initial activation of CO_2 on the electrocatalyst and their importance for understanding selectivity. Carbon–carbon bond formation is also a key mechanistic step in CO_2 electroreduction to high-density and high-value fuels. We show that both the initial CO_2 activation and C–C bond formation are influenced by an intricate interplay between surface structure (both on the nano- and on the mesoscale), electrolyte effects (pH, buffer strength, ion effects) and mass transport conditions. This complex interplay is currently still far from being completely understood. In addition, we discuss recent progress in in situ spectroscopic techniques and computational techniques for mechanistic work. Finally, we identify some challenges in furthering our understanding of these themes.

With the growing importance and falling prices of renewable electricity, the issue of electricity storage to deal with the intermittent nature of renewable energy sources is becoming urgent. Storing renewable electricity in chemical bonds ('electrofuels') is particularly attractive, as it allows for high-energy-density storage and potentially high flexibility. While hydrogen is the most likely and realistic candidate for electricity storage in electrofuels, research on the electrochemical conversion of carbon dioxide and water into carbon-based fuels has intrigued electrochemists for decades, and is currently undergoing a notable renaissance[1–4]. In contrast to hydrogen production by water electrolysis, carbon dioxide electrolysis is still far from a mature technology. Significant hurdles regarding energy efficiency, reaction selectivity and overall conversion rate need to be overcome if electrochemical carbon dioxide reduction is to become a viable option for storing renewable electricity.

Many electrocatalysts have been reported for the production of different compounds from the electrocatalytic carbon dioxide reduction reaction (CO_2RR). Table 1 gives an overview of some of the most active and selective metal or metal-derived electrocatalysts towards specific products in aqueous media. The two-electron transfer products, CO and HCOOH, can be produced with low overpotential and high Faradaic efficiency on suitable electrocatalysts, but substantially higher overpotentials and lower selectivities are observed for multi-electron transfer products such as methane, ethylene and alcohols[2]. For a recent discussion about the economic perspectives of CO_2RR, the reader is referred to a previous analysis[5].

The aim of this Review is not to be exhaustive, but rather to selectively (and subjectively) discuss some recent advances and pertinent challenges in this field, focusing on themes that have recently witnessed important progress[2,3,6,7]. An overview of some of the themes covered in this Review is shown in Fig. 1. We also discuss two important methodologies used to increase fundamental understanding of CO_2RR: in situ spectroscopic techniques and computational techniques.

Initial activation of CO_2

The first step in the CO_2RR is the activation of the CO_2 molecule. It is often claimed that activation and reduction of CO_2 is difficult because the first electron transfer to form the $CO_2^{\bullet-}$ radical intermediate has a very negative redox potential (−1.9 V versus normal hydrogen electrode), or because CO_2 is a very stable molecule[4]. Neither statement is accurate. Electrocatalysts stabilize the $CO_2^{\bullet-}$ radical or reaction intermediate by forming a chemical bond between CO_2 and catalyst, leading to a less negative redox potential. With the right electrocatalyst, it is possible to reduce CO_2 to CO or HCOOH at low overpotential. This low-overpotential reversible catalysis is related to the mechanism of a two-electron process, typically consisting of only one intermediate, which can be optimized using an appropriate catalyst[8,9]. Enzymes such as formate dehydrogenase and carbon monoxide dehydrogenase are indeed effective reversible catalysts for the CO_2RR to formate and carbon monoxide, respectively, exhibiting negligible overpotentials[10]. In addition, the equilibrium potentials of CO_2RR are close to 0 V (and sometimes higher), making the thermodynamic stability of CO_2 similar to that of water.

We consider four redox reactions related to the activation of CO_2 (equations (1)–(4)):

$$* + CO_2 + H^+ + e^- \rightarrow {}^*COOH \tag{1}$$
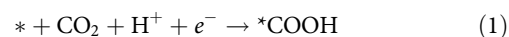
[1]Leiden Institute of Chemistry, Leiden University, Leiden, the Netherlands. [2]Present address: Separation and Conversion Technology, Flemish Institute for Technological Research, Mol, Belgium. [3]Present address: Department of Sustainable Process and Ene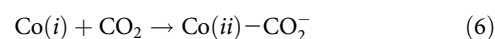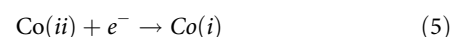rg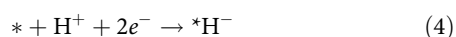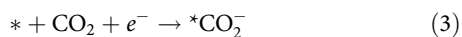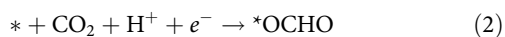y Systems, TNO, Delft, the Netherlands. [4]Present address: Department of Chemical Engineering and Chemistry, Eindhoven University of Technology, Eindhoven, the Netherlands. [5]Present address: Departament de Ciència de Materials i Química Física and Institut de Química Teòrica i Computacional, Universitat de Barcelona, Barcelona, Spain. *e-mail: f.calle.vallejo@ub.edu; m.koper@lic.leidenuniv.nl

Table 1 | Highly selective/active metal and metal-derived electrocatalysts for synthesis of specific CO₂RR products

CO₂RR product	Electrocatalyst	Faradaic efficiency (%)	η (V)[a]	j_{total} (mA cm⁻²)	Electrolyte (CO₂ saturated)	Ref.
HCOOH	Pb	97.4	−1.19 V	5.0	0.1 M KHCO₃[b]	[8]
	Sn	88.4	−1.04 V	5.0	0.1 M KHCO₃[b]	[8]
	Pd nanoparticles/C	99	−0.15 V	2.4–7.0	2.8 M KHCO₃[c]	[23]
	Pd₇₀Pt₃₀ nanoparticles/C	90	−0.36 V	4.0–7.5	0.2 M PO₄³⁻ buffer[d]	[9]
CO	Au	87.1	−0.64 V	5	0.1 M KHCO₃[b]	[8]
	Au nanoparticles	97	−0.58 V	3.49 ± 0.61	0.1 M KHCO₃[b]	[173]
	OD-Au nanoparticles	>96	−0.25 V	2–4	0.5 M NaHCO₃[e]	[103]
	Ag	94	−0.99 V	~5	0.1 M KHCO₃[b]	[174]
CH₄	Cu poly	40.4	−1.34 V	~7	0.1 M KHCO₃[b]	[55]
	Cu(210)	64	−1.29 V	5	0.1 M KHCO₃[b]	[33]
C₂H₄	Cu poly	26.0	−1.13 V	1–2	0.1 M KHCO₃[b]	[55]
	O₂ plasma-treated Cu	60	−0.98 V	~15	0.1 M KHCO₃[b]	[112]
	Cu-halide	60.5–79.5	−2.11 V	46.1–39.2	3 M KBr[f]	[83]
	Graphite/carbon NPs/Cu/PTFE	70	−0.63 V	75–100	7 M KOH[g]	[31]
CH₃OH	Cu₂O	38	−0.43 V	1–2	0.5 M KHCO₃[h]	[121]
	HCl-pretreated Mo	84	−0.33 V	0.12	0.2 M Na₂SO₄[i]	[175]
C₂H₅OH	Cu poly	9.8	−1.14 V	~0.6	0.1 M KHCO₃[b]	[55]
	Cu₂O	9–16	−1.08 V	30–35	0.1 M KHCO₃[b]	[123]
	CuO nanoparticles	36.1	NA[j]	~11.7	0.2 M KI	[124]
	Cu/CNS	63	−1.29 V	2	0.1 M KHCO₃[b]	[176]

[a]$\eta = E - E^0$ with E^0 versus RHE, where η is overpotential, E is applied potential and E^0 is standard electrode potential[6]. [b]pH ≈ 6.8. [c]pH ≈ 8.2. [d]pH ≈ 6.7. [e]pH ≈ 7.2. [f]pH ≈ 3. [g]pH > 14. [h]pH ≈ 7.6. [i]pH ≈ 4.2. [j]At E = −1.7 V versus saturated calomel electrode (pH not reported). j_{total}, total current density; NA, not available.

$$* + CO_2 + H^+ + e^- \rightarrow {}^*OCHO \qquad (2)$$

$$* + CO_2 + e^- \rightarrow {}^*CO_2^- \qquad (3)$$

$$* + H^+ + 2e^- \rightarrow {}^*H^- \qquad (4)$$

$$Co(ii) + e^- \rightarrow Co(i) \qquad (5)$$

$$Co(i) + CO_2 \rightarrow Co(ii) - CO_2^- \qquad (6)$$

Equations (1) and (2) are so-called concerted proton–electron transfer (CPET) reactions and have been considered computationally for deriving trends in selectivity among (post-)transition metal surfaces[11]. The authors argued that *COOH is the more likely first intermediate for CO formation, and *OCHO the more likely intermediate for formic acid production (an assertion that is generally agreed on in the literature). Using calculated binding energies, they generally find good agreement between their predictions and experiment: post-transition metals such as Pb and Sn prefer to bind CO₂ via oxygen and are selective towards formic acid, whereas transition-metal electrodes prefer to bind via carbon. Interestingly, in two instances, their calculations deviate from the experimental observations in Table 1: silver is predicted to be an excellent catalyst for formic acid production, whereas palladium is predicted to have the lowest onset potential for CO production. They ascribe these differences to kinetic effects not included in their calculations.

Interestingly, in the molecular electrocatalysis community, the views on the initial activation of CO₂ appear to be subtly different. The initial binding of CO₂ to the catalyst does not involve a CPET step such as in equations (1) and (2), but rather an electron-transfer mediated CO₂ binding step, as indicated by equation (3). The CO₂⁻ anionic adduct is generally bound to the metal centre of the catalyst. For instance, for a cobalt-(proto)porphyrin catalyst, CO₂ binding takes place if the cobalt centre changes oxidation state from Co(ii) to Co(i), with the electronic density flowing back onto the *CO₂ ligand, formally written as in equations (5) and (6).

Subsequent protonation or CPET steps generate *COOH or *COOH⁻ intermediates[12]. If equation (3) is rate determining or potential determining, the pH dependence of CO₂ activation may differ from the pH dependence of the competing hydrogen evolution reaction (HER). This different pH dependence of the CO₂RR and HER pathways was used to explain the strong pH dependence of the overall product selectivity on graphite-immobilized Co-protoporphyrin, with H₂ being the primary product at pH 1 but CO being the primary product at pH 3 (refs. [13,14]). A similar mechanistic model was proposed for gold-catalysed CO₂RR, suggesting that also on gold the *CO₂⁻ intermediate, and not *COOH, is the relevant activated form of CO₂ (ref. [15]). Recent computational work has confirmed that on Ag(111) *CO₂ is highly sensitive to the presence of an electric field, as, for example, modelled by the presence of a cation[16]. Although the authors do not write the formation of *CO₂ as an electron-transfer step, the resulting *CO₂ is highly polarizable, and therefore sensitive to pH and cation effects (see 'Reaction and process conditions'). Similar conclusions regarding the importance of a *CO₂^δ− intermediate in the CO₂RR reduction to CO on a Ag(110) electrode have been drawn based on kinetic simulations of CO formation using a multiscale model[17].

A similar situation exists for formate/formic acid production on molecular catalysts. Among metalloporphyrins, Rh, Sn and In protoporphyrins have a high selectivity towards formic acid in aqueous electrolyte[18]. Density functional theory (DFT) calculations suggest that the key intermediate is an anionic hydride[19], formed through equation (4), as previously suggested in the molecular catalysis
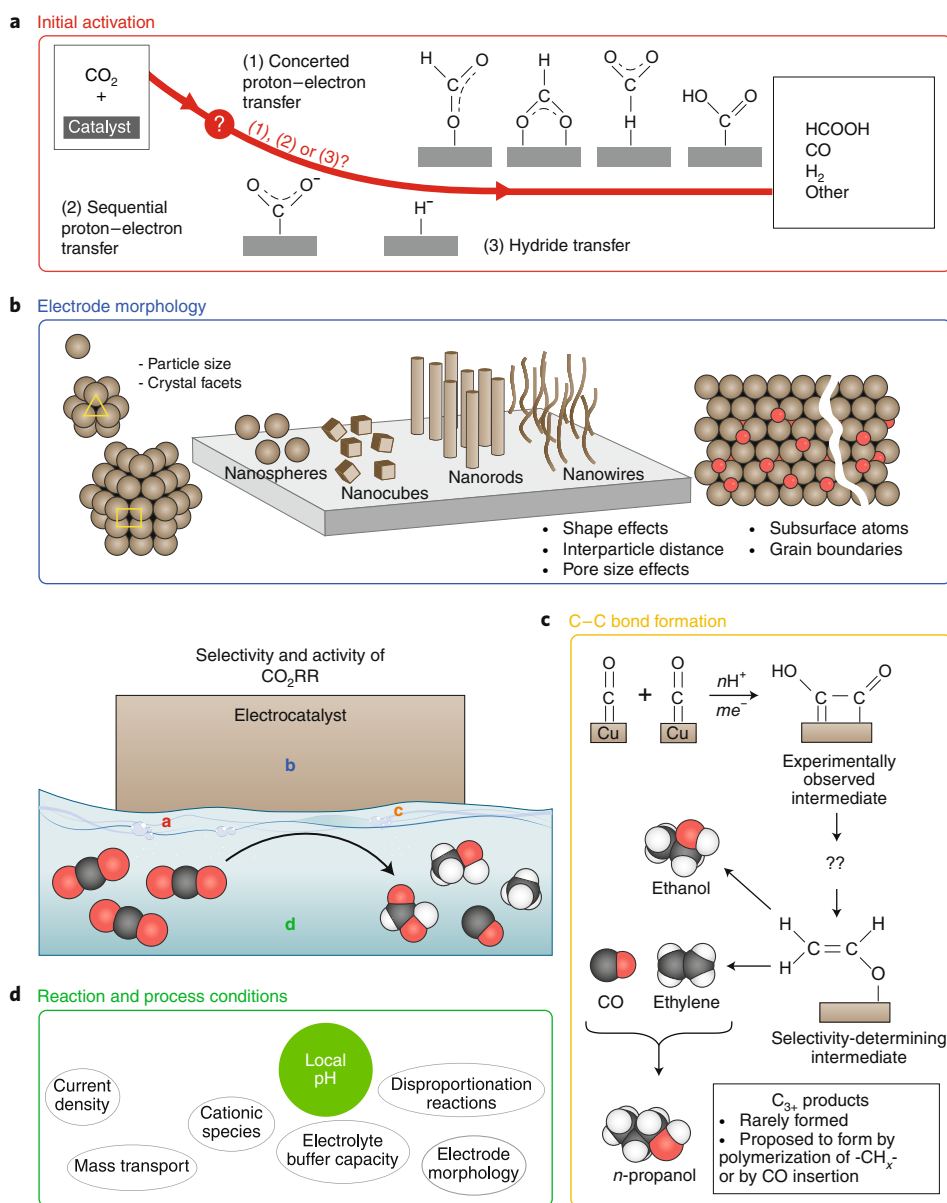
Fig. 1 | Overview of themes discussed in this review. a, Initial activation of CO_2, which can proceed via CPET, SPET or hydride-transfer mechanisms. **b**, Influence of the mesostructure of the electrode on the selectivity and activity of CO_2RR. **c**, Recent views on C–C bond formation from CO_2RR, specifically the formation of C_2H_4 and C_{3+} products. **d**, The important role of reaction and process conditions, such as local pH, on CO_2RR activity and selectivity.

literature[20,21]. The anionic hydride performs a nucleophilic attack on the carbon atom of CO_2, yielding $HCOO^-$. Again, the reaction is triggered by a potential-induced change in the oxidation state of the catalyst, either of the metal centre or the ligand, with the hydride residing on the metal or the ligand (the latter is the most likely pathway for In and Sn porphyrins). The stability of the resulting species is crucial to the subsequent elementary step and the formation of either CO or $HCOOH/HCOO^-$. Interestingly, such a (lattice-)hydride mechanism was recently proposed for nanostructured copper-hydride catalysts with a much enhanced selectivity for formic acid ('normal' copper yields primarily CO as a two-electron product)[22]. The importance of a hydride-mediated pathway has also been suggested for formate production on palladium electrodes, as well as in solution[23,24].

The relevance of considering equations (3) and (4) in the activation of CO_2 as opposed to equations (1) and (2), is that the intermediates involved are charged (or strongly polarizable) and hence

sensitive to pH and cation effects. A summary of the discussed activation routes for CO_2RR is given in Fig. 2.

Carbon–carbon bond formation

One of the most interesting observations in the CO_2RR is the formation of species with one or more carbon–carbon bonds, mostly on copper-based electrodes. Apart from copper-based catalysts, a few others, for example, NiGa, PdAu, NiP and N-doped carbon catalysts, produce compounds with two or more carbon atoms, but not with the same efficiency as copper[25–28]. There have been some remarkable achievements recently in terms of improving selectivity to C_2 compounds by tuning copper structure (for example, using high-surface-area oxide-derived (OD) copper), by adjusting electrolyte composition and by employing organic films on copper[29–32].

The interest in making more reduced (liquid) products from CO_2 lies in the fact that they have higher energy density and economic value[5]. Therefore, elucidating the pathway(s) from CO_2 or CO to
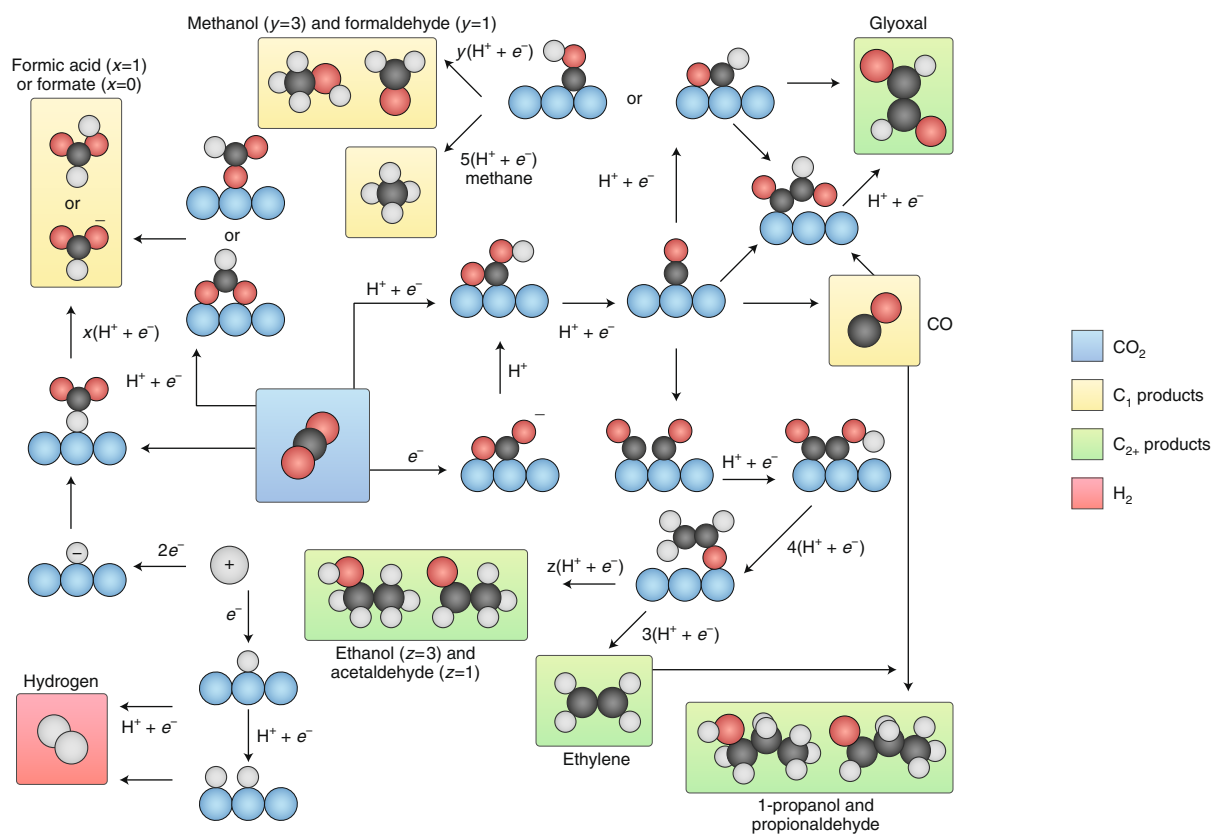
Fig. 2 | Overview of reaction pathways for CO$_2$RR towards different products. Black spheres, carbon; red spheres, oxygen; white spheres, hydrogen; blue spheres, (metal) catalyst. The arrows indicate whether proton, electron or CPETs take place.

C$_2$ products, of which ethylene and ethanol are the most typical examples, has been the subject of several experimental[33–38] and theoretical[39–43] studies. Two separate pathways for ethylene production have been observed experimentally: a high-overpotential pathway involving a shared intermediate with the methane pathway taking place primarily on Cu(111), and a low-overpotential pathway taking place primarily on Cu(100) and which does not yield C$_1$ products[36]. The two pathways also differ in the their pH dependence: the 'Cu(111) pathway' is pH dependent (on the normal hydrogen electrode potential scale), whereas the 'Cu(100) C$_2$ pathway' is not. As a result, the latter pathway is favoured over the former pathway, and over hydrogen evolution in alkaline media, making the selectivity of the CO$_2$ and CO reduction on copper highly sensitive to (local) pH. Several experimental[34,37] and theoretical[39–41] studies have suggested a CO dimer intermediate as the key species in this C$_2$ pathway. DFT calculations show that at more negative potentials, CO dimerization is disfavoured and that an alternative reaction pathway based on the coupling of *CO and *CHO has a lower activation energy[41,44]. Both experiments and DFT calculations suggest that the rate-determining step in C–C coupling involves a decoupled proton–electron transfer[39], explaining its pH sensitivity. DFT calculations also show that the CO dimer is energetically favoured in the presence of a water layer, a local electric field and alkali cations, and that its formation energy is most favourable on Cu(100) (refs. [40,42]), in agreement with the experimental observation that it is a structure-sensitive and pH-sensitive reaction. Recently, evidence has been provided for a hydrogenated CO dimer intermediate (OCCOH) at low overpotentials in alkaline LiOH electrolyte during CO reduction using Fourier transform infrared spectroscopy, supported by DFT calculations[45]. Its formation was only observed on Cu(100) and not on Cu(111), in agreement with previous studies[35,42]. Interestingly,

ethylene formation is favoured in Cs$^+$-containing electrolyte, both during CO$_2$ and CO reduction, although the alleged dimer intermediate was not observed in CsOH electrolyte, presumably because it is more reactive. Copper modified with certain organic layers also shows improved selectivity to C$_2$ products[29,30]. These effects are not fully understood yet but may be related to local pH effects. It is well known that 'designing' an electrolyte that allows for a high near-electrode pH during CO$_2$RR, such as a low buffer strength electrolyte, leads to enhanced C$_2$ production[46].

Besides ethylene, other C$_2$ products observed during CO$_2$ and CO reduction on copper are acetaldehyde and ethanol. It is normally assumed that these C$_2$ species are formed through common intermediates on Cu(100) up to a selectivity-determining intermediate, the hydrogenation of which leads to acetaldehyde and subsequently ethanol, and the hydrogenolysis of which leads to ethylene[39]. We have proposed that *CH$_2$CHO could be such an intermediate[47,48]. The structure sensitivity of the further reduction of this intermediate then determines the dominant C$_2$ product, ethylene or ethanol[47–49]. However, recent computational work suggested that the selectivity-determining intermediate is formed earlier in the mechanism[44]. An alternative pathway for ethanol formation was suggested, claiming that on CuZn or CuAg an insertion-type mechanism (CO reacting with Cu–CH$_2$ species) is operative[50]. We note that the CO dimerization mechanism can also explain why silver produces small amounts of ethanol (and no ethylene)[47]. Acetate is another frequently observed C$_2$ product. It has been proposed to form as a by-product in the reaction path towards ethylene via isomerization of a three-membered ring species adsorbed on the surface (*OCH$_2$COH) as well as through the coupling of different adsorbed intermediates[51,52]. However, acetate has been shown experimentally to form in solution as a result of a base-catalysed

disproportionation of acetaldehyde[53]. As far as we know, this is the only pathway that can explain why acetate can be formed also during CO reduction. An overview of reaction pathways towards C_{2+} products is shown in Fig. 2, with the important caveat that it seems probable that several competing pathways are operative, in particular at large overpotentials.

The formation of higher-order (C_{3+}) hydrocarbons has also been observed on copper, with a Faradaic efficiency of up to 20% on a suitable copper catalyst.[54] The main C_3 products are propanol and propionaldehyde, with small amounts of hydroxyacetone, acetone and allyl alcohol[55]. The elementary steps through which these C_3 products are formed have not been well studied yet. C–C coupling between CO and C_2H_4 precursors has been reported to form n-propanol on agglomerates of OD copper nanocrystals[56]. For this reaction, defect sites were proposed to be the active sites. Moreover, polymerization of adsorbed carbon-based species has been proposed as a mechanism for the formation of higher-order hydrocarbons on bimetallic PdAu electrodes[26]. Although CO insertion-type reaction steps seem likely, there is still a lack of mechanistic work on the electrochemical formation of C_{3+} hydrocarbons.

Reaction and process conditions

The nature of the solvent (aqueous or non-aqueous), pH, the identity of ionic species, buffering strength and the exact mass-transport conditions all influence the activity and selectivity of CO_2RR[57]. However, the interpretation of the individual effects remains poorly understood, and only recently systematic work was performed to elucidate and separate these effects. The importance of reaction and process conditions also implies the importance of proper standard protocols, as discussed recently[58].

The CO_2/HCO_3^-, H_2CO_3/HCO_3^- and HCO_3^-/CO_3^{2-} equilibria in water are sensitive to (bulk) pH, electrolyte composition and buffer capacity, which leads to different concentrations of carbonaceous species in solution (Fig. 3a)[59]. This has led to some controversy about the real active form of CO_2 during CO_2RR. Most authors acknowledge now that dissolved CO_2 is the active species, though bicarbonate has also been suggested as the active species, especially towards formate[60–62]. Enhanced CO_2RR activity in bicarbonate electrolyte, compared with other electrolytes under similar conditions, has been proposed to be associated with the formation of a bicarbonate–CO_2 complex. Such a complex is a primary carbon source during CO_2RR, leading to an increase in CO_2 concentration in the vicinity of the electrode[63]. In situ Fourier transform infrared experiments using isotope labelling have confirmed this role of bicarbonate[64]. However, it was concluded that bicarbonate is not explicitly involved as an active species in the rate-limiting step of CO formation on gold, but rather that bicarbonate is a proton donor in a reaction step after the rate-limiting step[65]. The authors also conclude that the sluggish kinetics of the reaction converting bicarbonate into CO_2 must be considered. More generally, buffering anions in the electrolyte can donate a proton more effectively than water, or compared with other anions, which leads to an anion effect for the HER and formation of CH_4, but not for CO_2RR towards CO, $HCOO^-$, C_2H_4 and ethanol[66].

As soon as Faradaic currents are flowing, the importance of the local pH and local concentration of carbonaceous species must be taken into account[46,57,67,68]. The interpretation of experimental data must invoke the presence of local concentration gradients[68]. During CO_2RR, a more alkaline pH than the bulk pH is manifested in the vicinity of the electrode, as a result of hydroxide formation from both the HER and CO_2RR. This local alkaline pH is the result of mass-transport limitations[57]. This local pH change is proportional to the current density[69], but also depends on the nature and buffer capacity of the electrolyte, and on the morphology of the electrode. Therefore, modelling concentration gradients near the electrode surface during CO_2RR is crucial to understand the overall reactive system. Recent

model calculations of pH gradients and CO_2 transport within a fixed boundary layer for different electrolytes showed the importance of buffer identity, buffer capacity, buffer pK_a and CO_2 pressure on the reaction kinetics, as well as the importance of the buffer kinetics[70]. We expect that the combination of such models with surface kinetics models will become increasingly important in designing reactive electrochemical three-dimensional interphases as shown in recent work on pH effects to explain C_1 versus C_2 selectivity[71].

Since the (local) pH near the electrode has such an important role in some of the crucial steps in CO_2RR (see the previous sections), reactivity and selectivity can be tuned by the electrolyte composition[46,67,70]. A prime example of this effect happens on Cu electrocatalysts, for which the selectivity towards ethylene can be enhanced by lowering the buffer capacity, thereby favouring a higher local pH[46,72]. In addition, the selectivity can be steered towards ethylene by increasing the CO_2 pressure, leading to enhanced local CO concentration and a higher *CO coverage[71].

Another parameter influencing the local pH and consequently the product distribution of CO_2RR is the electrode morphology (Fig. 3c). It has been shown that the increased mesoporosity of silver and gold catalysts alters the selectivity in favour of CO_2-to-CO conversion, compared with H_2 evolution, which is attributed to enhanced local pH gradients in highly mesoporous films[73,74]. These trends were corroborated by comparison to rotating (cone) electrode experiments, showing that enhanced mass transport is advantageous to hydrogen evolution, but has a neutral or inhibitive effect on CO_2RR. Using rotating copper cylinder electrodes, it was shown that the CO_2RR activity decreases with higher rotation rate, related to a change in selectivity from CH_4 to CO as CO is more readily transported away with enhanced convection[75]. Rotating copper disk electrode experiments in mildly acidic media revealed that water reduction is the HER pathway in competition with CO_2RR, instead of proton reduction[76]. The suppression of water reduction on copper was suggested to be the result of *CO on the copper electrode, which is more pronounced at low rotation rates (as CO does not diffuse away). Note that one should be careful with the interpretation and comparison of experimental data of high-surface-area electrocatalysts on the reversible hydrogen electrode (RHE) scale, since the local pH may be significantly different compared with the bulk pH, leading to deviations on the RHE scale[58].

Another consequence of a local alkaline pH as a result of the concomitant HER during CO_2RR is the occurrence of homogeneously catalysed chemical reactions, which may seriously affect the overall product spectrum[53,77]. Cannizzaro-type reactions can take place during CO_2RR, in which intermediate aldehydes disproportionate into their corresponding carboxylic acid and primary alcohol[53]. This phenomenon is enhanced by the alkaline pH near the electrode, and is therefore more important in poorly buffered or unbuffered electrolytes, and on electrodes with high porosity. The obtained products (acids and alcohols) should be distinguished from direct CO_2RR products.

The nature of the electrolyte cations and anions has been shown to have a significant effect on the activity and selectivity of the CO_2RR. Larger cations usually lead to higher CO_2RR rates and a higher C_2/C_1 ratio (on copper electrodes)[78–80]. A cation hydrolysis effect has been suggested to lead to an enhanced buffering near the electrode for larger cations, which in turn increases the local concentration of dissolved CO_2 (refs. [79,81]). An alternative rationalization of the cation effect is the lesser stabilization of 2 *CO compared with *OCCO and *OCCOH (refs. [16,32,82]). The onset potential for ethylene depends on the cation nature, while for methane no correlation with cation size was found[82].

The effect of anions on the CO_2RR has been investigated, although less extensively compared with cations, and these studies generally deal with halide effects on copper[83–87]. Anion effects are generally explained in terms of halide adsorption on the catalyst
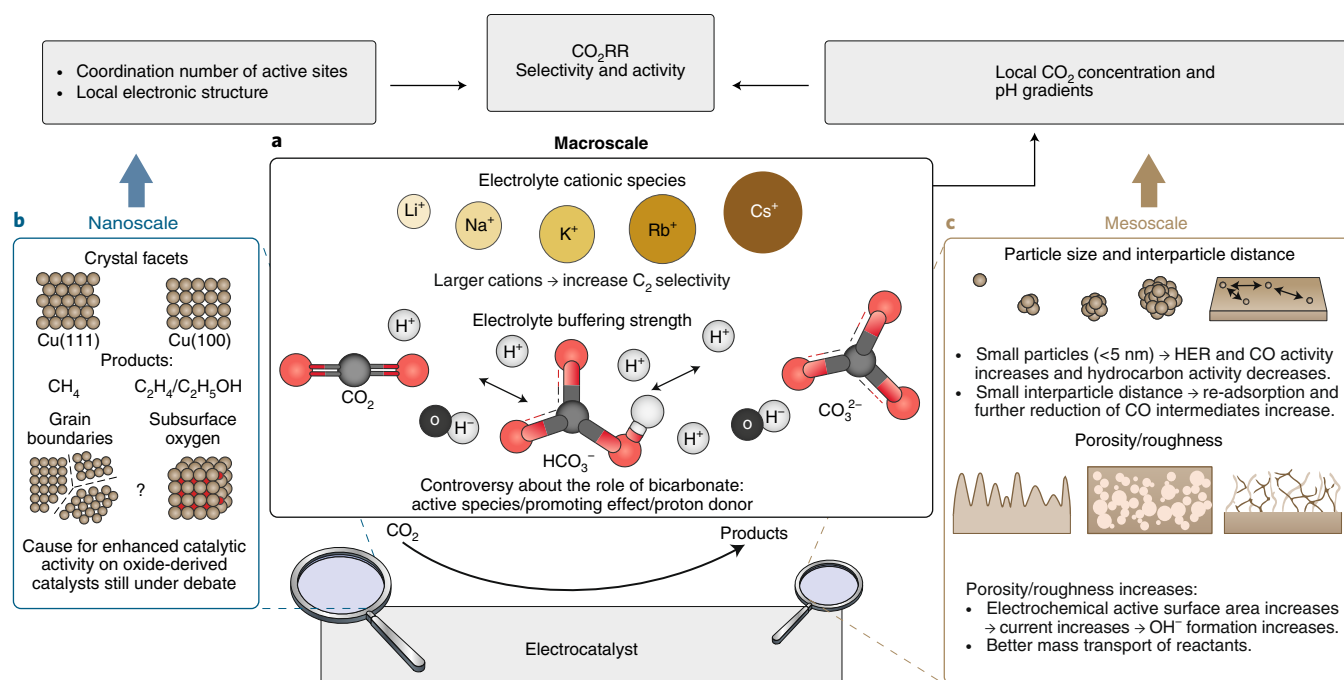
Fig. 3 | Schematic of the different length scales involved in the understanding of CO₂RR and of the influence of relevant parameters. a, Macroscale: electrolyte composition and buffering strength. **b**, Nanoscale: crystal facets, grain boundaries or subsurface oxygen. **c**, Mesoscale: influence of particle size, interparticle distance and porosity.

surface, altering the electronic structure and subsequently the CO₂RR activity and selectivity, which are also dependent on the halide size and concentration[85]. Moreover, specifically adsorbed halide anions can suppress proton adsorption, favouring CO₂RR with respect to the HER[84]. Halide ions can also aid in the formation of well-defined copper nanocrystals by nanostructuring of the copper catalyst[86]. As mentioned before, buffering anions have also been shown to have a role in the formation of H₂ and CH₄ (ref. [66]).

Electrode morphology and (sub)surface atoms
The effect of electrode morphology on CO₂RR performance should be understood on different length scales, a schematic illustration of which is shown in Fig. 3. On one end of the spectrum is the atomic-level structure of the surface, which can be studied with different single-crystal surfaces (Fig. 3b)[33]. Nanostructured[88–92] and meso-structured[74,93–96] catalysts and OD electrodes[97–105] have been shown to influence the CO₂RR activity and selectivity through the variation of the coordination number of the active sites, local electronic structure by the presence of subsurface oxygen, catalyst particle size and readsorption of intermediates by the interparticle distance. The electrode's mesostructure also substantially affects the mass transport of reactants (Fig. 3c). Rough or high-surface-area surfaces, such as OD copper electrodes, exhibit improved hydrocarbon selectivity compared with smooth surfaces. This is typically attributed to the increased population of undercoordinated sites[88], but as discussed in the previous section, high-surface-area mesoporous catalysts also tend to suppress hydrogen evolution due to the poorer mass transport in porous systems. Cubic-shaped copper nanocrystals steer the selectivity towards ethylene with respect to methane[89,90], in agreement with the observation that Cu(100) facets favour C–C coupling.

A particle size effect of Cu nanoparticles has been reported[92], showing that the activity for H₂ and CO is increased with decreasing particle size (<5 nm), while the selectivity towards hydrocarbons is decreased. This observation was attributed to a higher number of undercoordinated sites (coordination number < 8), which promote HER and CO formation due to stronger chemisorption of *CO.

Paradoxically, *CO is difficult to be reduced further, which was ascribed to lower surface mobility. Particle-size effects of CO₂RR activity on gold nanoparticles have also been observed, leading to a drastic increase in the H₂/CO ratio for very small nanoparticles, which was attributed to the increase of specific edge sites that enhance *COOH stabilization with respect to *H stabilization[106,107].

Investigation of mesoscale phenomena has also demonstrated the effects of particle size and particle distance on the product selectivity for well-defined Cu catalysts[95]. Re-adsorption of CO intermediates, followed by their further reduction, was found to be associated with small interparticle distance and larger nanoparticle sizes, whereas small nanoparticles suffer from active-site poisoning by CO.

Various authors have suggested pre-treatments of (metallic) catalysts to enhance their activity for CO₂RR. Increased efficiency, selectivity and stability of CO₂RR were revealed on OD electro-catalysts, which were obtained by reducing metal-oxide films[97,103]. Improved CO₂RR activity has been reported for OD-Au, OD-Cu, OD-Ag and OD-Pb[97,98,103–105]. Many papers have been published regarding CO₂/CO reduction on OD-Cu electrodes[99–102], but the key factors responsible for the improved selectivity and activity of OD electrocatalysts are still debated. In this respect, increased stabilization of the CO₂ anionic adsorbate (CO₂•⁻) by grain boundaries as well as the presence of (sub)surface oxygen have been reported to play a role, although no consensus has been reached yet[108–110].

On OD-Au, a high selectivity to CO at low overpotential was found, which was ascribed to improved stabilization of CO₂•⁻ on OD-Au compared with polycrystalline Au[103]. Grain boundaries have also been shown to have enhanced activity for CO₂RR activity on Au[111]. Similar conclusions have been drawn regarding CO production on OD-Cu[100]. In addition, on oxide-derived copper the enhanced activity and stability compared with polycrystalline copper depend on the initial thickness of the Cu₂O layers and is not significant for thin films (<3 μm)[97,101]. Remarkable improvements of the selectivity towards ethanol, acetate and n-propanol for CO reduction on similar OD electrodes have been reported[102], with the improved selectivity attributed to grain boundaries.

Oxygen plasma activation is another form of pretreatment that yields significantly enhanced CO_2RR activity[112,113]. The treatment is suggested to yield highly defect-rich surfaces. In the case of plasma-treated copper, subsurface oxygen and the presence of Cu^+ have been suggested as key for the reactivity and selectivity enhancement. Following up on the potential involvement of subsurface oxygen, it was proposed that it modifies the electrocatalyst's electronic structure by reducing σ-repulsion, leading to increased *CO binding energies, primarily near grain boundaries[110]. Another explanation is that subsurface oxygen facilitates neutral and charged copper sites at the surface, leading to chemisorbed CO_2 in presence of water and consequently enhanced CO_2RR activity[114]. DFT calculations have indeed shown that interstitial oxygen species are stable at the Cu(111) subsurface, contrary to Cu(211), and are capable of improving CO_2 binding to the surface[115]. In contrast, recent DFT-based work concluded that diffusion barriers for subsurface oxygen are low and hence it is unlikely that subsurface oxygen is stable during the negative potentials at which CO_2RR takes place[116]. From experiments employing ^{18}O labelling, it was also concluded that residual (subsurface) oxides should be unstable under CO_2RR conditions[117]. Moreover, theoretical work has shown that subsurface oxygen is not a prerequisite for CO_2 adsorption[118] and that coordinatively unsaturated Cu atoms facilitate C–C bond formation[42,119,120].

When Cu_xO is used directly for CO_2RR, methanol[121,122], ethanol[123,124] and ethylene[123] are observed as major products. It is often assumed that during CO_2RR, the Cu_xO electrocatalyst should be completely converted to metallic Cu. However, a residual oxide layer was shown to remain present on the surface during CO_2RR and the surface oxide and OD metallic layer were proposed as key reaction sites for catalysis[125]. The formation of $C_3–C_4$ products was also reported, supposedly due to a synergistic effect between Cu_2O and Cl adsorption, which resulted in a higher population of Cu^+ species[126]. In an interesting pulse voltammetry experiment, it was shown that a freshly oxidized copper electrode obtained by repeated anodic pulsing has enhanced selectivity towards oxygenated hydrocarbons[127].

In conclusion, the exact nature of the active sites of OD CO_2RR catalysts remains controversial and as yet unresolved. Apart from chemical or materials-related aspects such as those discussed, some researchers have argued that the activity and selectivity follow rather simple and consistent trends with current and potential[128]. Reliable methods to measure accurately the electrochemically active surface area[129] of copper electrodes (beyond surface capacitance measurements, which may sometimes be inaccurate[130]) will be paramount in clarifying such effective-surface-area effects.

In situ spectroscopic investigation of CO_2 reduction

There has been a number of recent in situ (or operando) spectroscopy studies of the CO_2RR, based on (surface-enhanced) infrared adsorption spectroscopy ((SE)IRAS) or surface-enhanced Raman spectroscopy (SERS). Such studies typically aim at identifying surface-adsorbed intermediates, and their observation or evolution as a function of parameters such as electrode potential, electrode surface and electrolyte composition.

SEIRAS was utilized to measure adsorption profiles of CO on copper electrodes[38]. *CO was observed at potentials $<−0.60$ V versus SHE, with a maximum coverage at ca. $−1.2$ V versus SHE, independent of pH. *CO was observed to be in dynamic equilibrium with CO in solution, and *CO is assumed to serve as a pool of intermediates for further reduction. In addition to *CO, other researchers also observed *H using SEIRAS, and demonstrated that the two species show an asymmetric blocking effect: *H can displace *CO, but *CO cannot displace *H (ref. [131]). Using isotope labelling and in situ SEIRAS, it was shown that carbonate is an important source of CO_2 near the electrode surface, implying a dynamic equilibrium between bicarbonate and dissolved CO_2 (ref. [64]). The authors also observed (very) weak bands possibly due to other surface-adsorbed intermediates such as *CHO or *COOH. Using both SEIRAS and SERS, the potential dependence of two different *CO bands was analysed, from which it was concluded that the copper surface undergoes a reversible morphological change during potential cycling[132]. The role of metastable surface oxides for CO_2RR was investigated on tin, indium, lead and bismuth electrodes, by means of attenuated total reflectance SEIRAS[133]. The results indicate the competition between CO_2 and H^+ for reaction sites (oxidized or metallic), depending on the nature of the electrode. Regarding the formation of C_2 species, our group used in situ IRAS on copper single-crystal electrodes to provide evidence for a (hydrogenated) dimer intermediate (*COCOH) with two different C–O stretching frequencies on Cu(100) in alkaline media, coinciding with the conditions under which CO reduction on copper yields C_2 products such as ethylene[45]. A recent theoretical work attributes those frequencies to different intermediates[134].

Following the previous discussion on the importance of local pH, in situ SEIRAS was used to probe the local pH by comparing the band intensities of HCO_3^- and CO_2, showing that the local pH near gold electrodes depends on the nature of the electrolyte cation[135]. SEIRAS was used on gold electrodes to study the production of CO (by adsorbing the CO generated at higher potentials) and showed the importance of HCO_3^- in effectively increasing the CO_2 concentration[63], as later confirmed for copper electrodes[64] (see previous paragraph).

Using in situ IRAS and SERS, a high sensitivity of CO_2RR in non-aqueous solvents to the presence of residual water has been observed[136]. In non-dry conditions, *CO is the major product at low overpotentials, and (bi)carbonates are formed at Cu, Pt, Au, Pd and Ag electrodes from the chemical reaction of CO_2 with OH^- species generated by water reduction. As a consequence, (bi)carbonate formation was found to be related to the water content. The formation of oxalate was observed only for Pb electrodes at high overpotentials.

As is customary with steady-state spectroscopy, identifying (low-coverage) reactive intermediates is difficult, and there is little consistent and widespread evidence for carbon-based intermediates other than *CO. Hyphenation of in situ spectroscopy with online product identification techniques would be a next instrumental challenge in furthering our understanding of CO_2RR, as it would enable the establishment of direct relationships between observed adsorbed intermediates and product selectivity. Moreover, in situ synchrotron-based techniques such as X-ray absorption spectroscopy[112,137] and ambient-pressure X-ray photoelectron spectroscopy[110] are promising in understanding interfacial electrochemistry, and have recently been employed to gain insight into the chemical state of the active (Cu) species on OD catalysts for CO_2RR. An overview of typical spectroelectrochemical techniques used for the understanding of CO_2RR is depicted in Fig. 4. For more elaborate reviews of in situ spectroelectrochemical techniques applied to CO_2RR research, the reader is referred to specialized recent reviews[138–140].

Computational approaches for CO_2 reduction

DFT calculations applied to the electrode/electrolyte interface are a far from simple endeavour, but much progress has been made in improving models. A recent detailed review of the computational modelling of CO_2 and CO reduction to (oxygenated) hydrocarbons can be found elsewhere[141]. Here we limit ourselves to the foundations, recent advances and key scientific challenges of descriptor-based analyses, which are the most widespread computational approaches for CO_2RR. An overview of the fundamentals of the method is depicted in Fig. 5.

The computational hydrogen electrode (CHE) is widely employed in computational electrocatalysis[142]. In combination with DFT-calculated adsorption energies of the intermediates (Fig. 5a), one
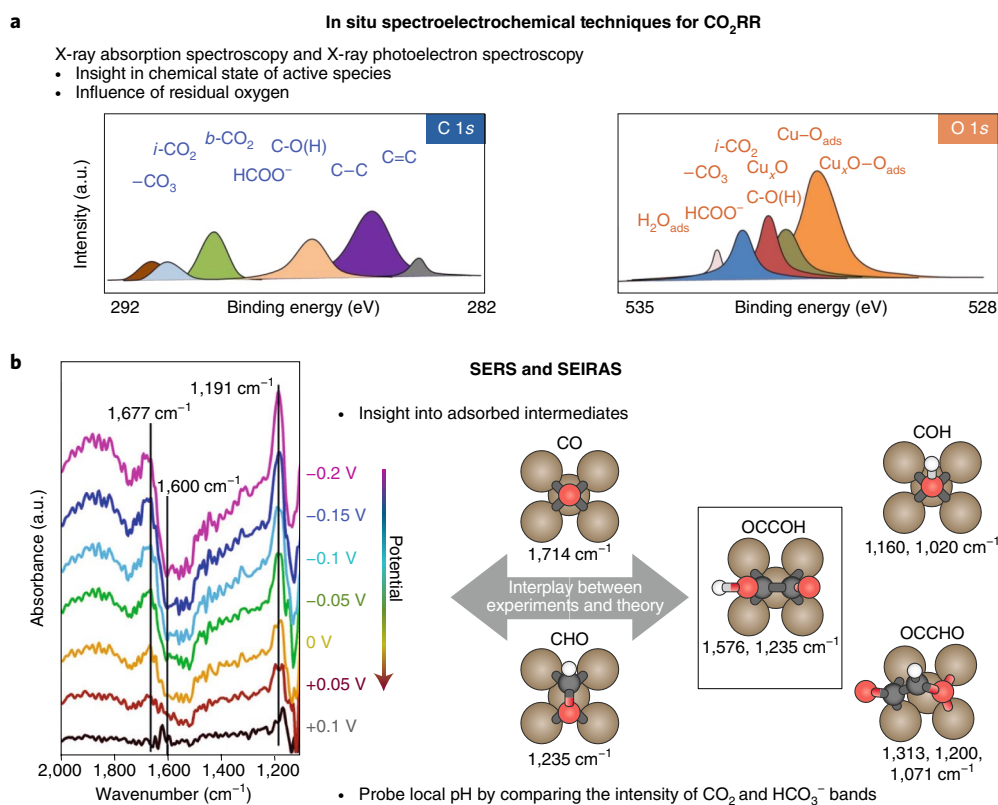
Fig. 4 | In situ spectroelectrochemical techniques used in the understanding of CO₂RR. a, X-ray absorption spectroscopy and (ambient-pressure) X-ray photoelectron spectroscopy to gain insight into the active species. **b**, SERS and (SE)IRAS for understanding the mechanism by observation of adsorbed intermediates (data reproduced from ref. [45] for the detection of OCCOH at low overpotentials during CORR in LiOH solutions), or to probe the local pH. Figure adapted from ref. [45], Wiley.

can gain insight into the coverage of surface species at specific pH and potentials by means of surface Pourbaix diagrams (Fig. 5b)[143], and possible reaction pathways and the potentials at which the redox reactions take place (Fig. 5c)[39,144,145]. Studies combining these approaches can also be found in the CO₂RR literature[146,147].

CHE-based models typically assume CPET steps, and are therefore not straightforwardly applicable for reaction pathways where decoupled proton–electron transfer steps are involved. Sequential proton–electron transfer (SPET) steps have been observed on molecular, oxide and metal electrocatalysts, and manifest experimentally through pH effects on the RHE scale[6,148,149]. Recently, a simple methodology was introduced that allows the transition between coupled and decoupled proton–electron transfer pathways to be predicted[12] based on first-principles calculations of acid–base equilibrium constants. Using this methodology, the experimental pH dependence of CO₂RR on immobilized cobalt protoporphyrins was rationalized, as discussed in the section about initial activation of CO₂ (ref. [13]).

The presence of linear correlations between adsorption energies of similar adsorbates, known as scaling relations (Fig. 5d)[150], reduces the complexity of DFT-based catalytic models and facilitates the simultaneous analysis of numerous materials through Sabatier-type activity plots (Fig. 5e). Such correlations per se do not carry information on the effect of applied potential, so it might be advisable to ascertain first the relevant surface coverage using surface Pourbaix diagrams[146,147]. Scaling relations might pose extra constraints for finding optimal electrocatalysts with low overpotentials, and have therefore been extensively studied[151–153]. Recent efforts were directed to break or circumvent scaling relations, especially between the intermediates of the electrocatalytic oxygen evolution

and reduction reactions and CO₂RR[42,154,155]. The strategy is clear, although difficult to implement experimentally: one of the problematic intermediates needs to be significantly stabilized with respect to the other(s). For instance, the preference of Cu(100) for the production of ethylene and ethanol over methane has been explained on the basis of the breaking of scaling relations between *CO and *CO dimers (*C₂O₂) on that facet due to strong ensemble effects for the CO dimerization step (Fig. 5d, top)[42]. Another example is the nearly reversible reduction of CO₂ to CO on CODH enzymes, the active site of which does not obey the scaling relationship between *CO and *COOH[156]. Furthermore, several strategies for breaking scaling relations in CO₂RR have been discussed: alloying, tethering, addition of promoters, creation of low-coordination sites and introduction of p-block dopants or oxophilic sites.[145,157] Other ways to depart from scaling relations are altering adsorbate solvation via modification of the electrolyte composition/dielectric constant[154,158], anchoring active ligands on the surface or at the active sites[159], strain effects[160] and the study of transition-metal-free electrocatalysts[147].

However, a word of warning is provided here. Recent studies have pointed out that breaking scaling relations is a necessary yet insufficient condition for the optimization of electrocatalysts. In other words, materials that break scaling relations are not necessarily active, while high activities can be achieved by materials that do not break them[153]. Furthermore, scaling-relation-based volcano plots for CO₂RR assume that a single mechanism is operative on all materials and facets (Fig. 5c,e)[145,157]. However, recent studies have shown that the CO₂RR reaction mechanism is both material and structure sensitive. For instance, while it is typically assumed that *CO hydrogenation leads only to *CHO, structure-sensitive scaling relations show that it may lead to *COH, *CHO, or both, depending
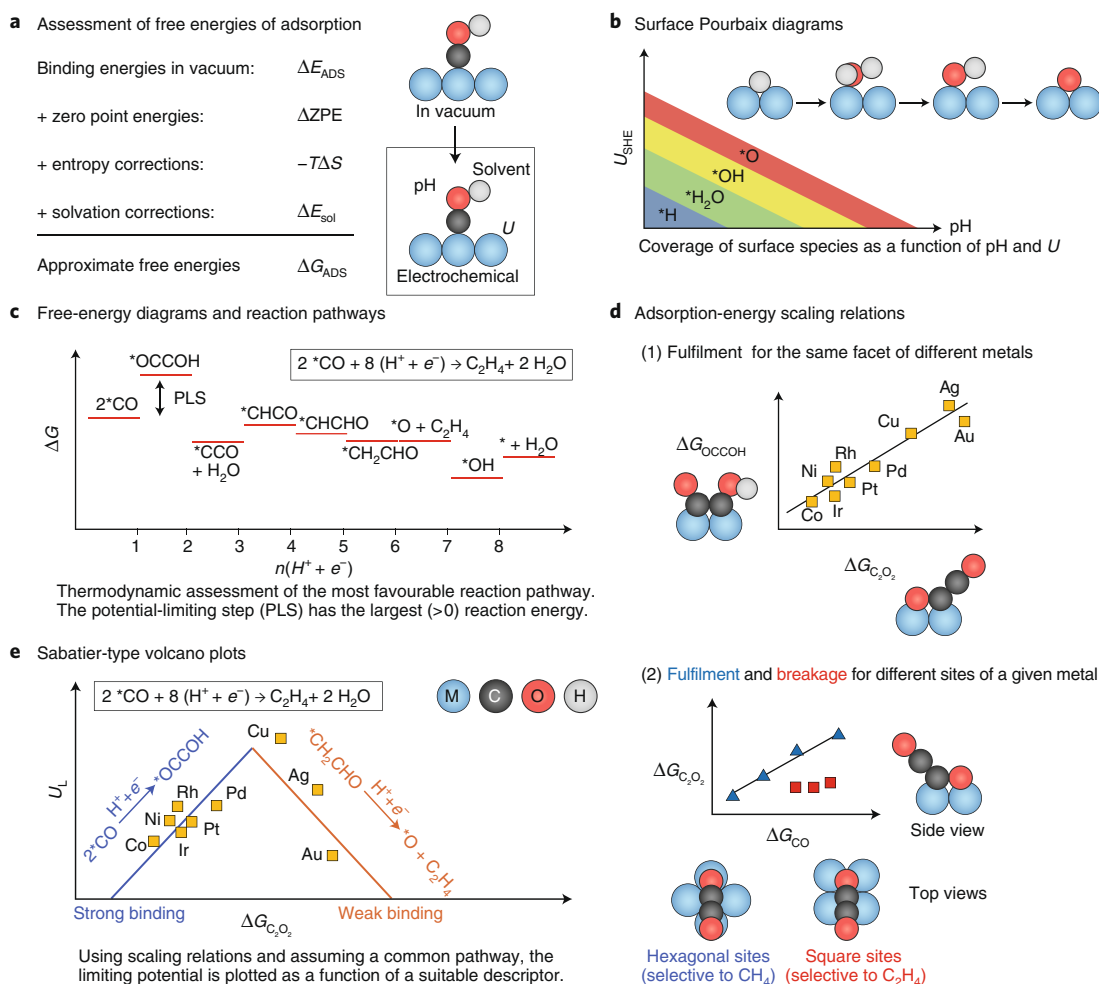
Fig. 5 | Fundamentals of descriptor-based analyses for CO₂RR. a, Assessment of free energies of adsorption starting from DFT calculations and adding zero-point energy, entropy and solvation corrections. **b**, Surface Pourbaix diagrams, which predict the thermodynamically most stable adsorbed species and their coverage as a function of pH and the potential versus the standard hydrogen electrode (U_{SHE}). **c**, Free-energy diagrams and most favourable reaction pathways for CORR to C_2H_4 on Cu(100). **d**, Various types of scaling relations between adsorption energies. **e**, Sabatier-type volcano plots based on scaling relations and the most favourable reaction pathway found in **c** for CORR to C_2H_4 on (100) surfaces of transition metals. The colour code is provided as an inset and M is a surface metal atom. Panels adapted from: **c**, ref. [39], Wiley; **d**, ref. [42], American Chemical Society; **d,e**, ref. [47], American Chemical Society.

on the active sites (Fig. 6a)[161] . Thus, such assumptions may sometimes lead to erroneous design principles.
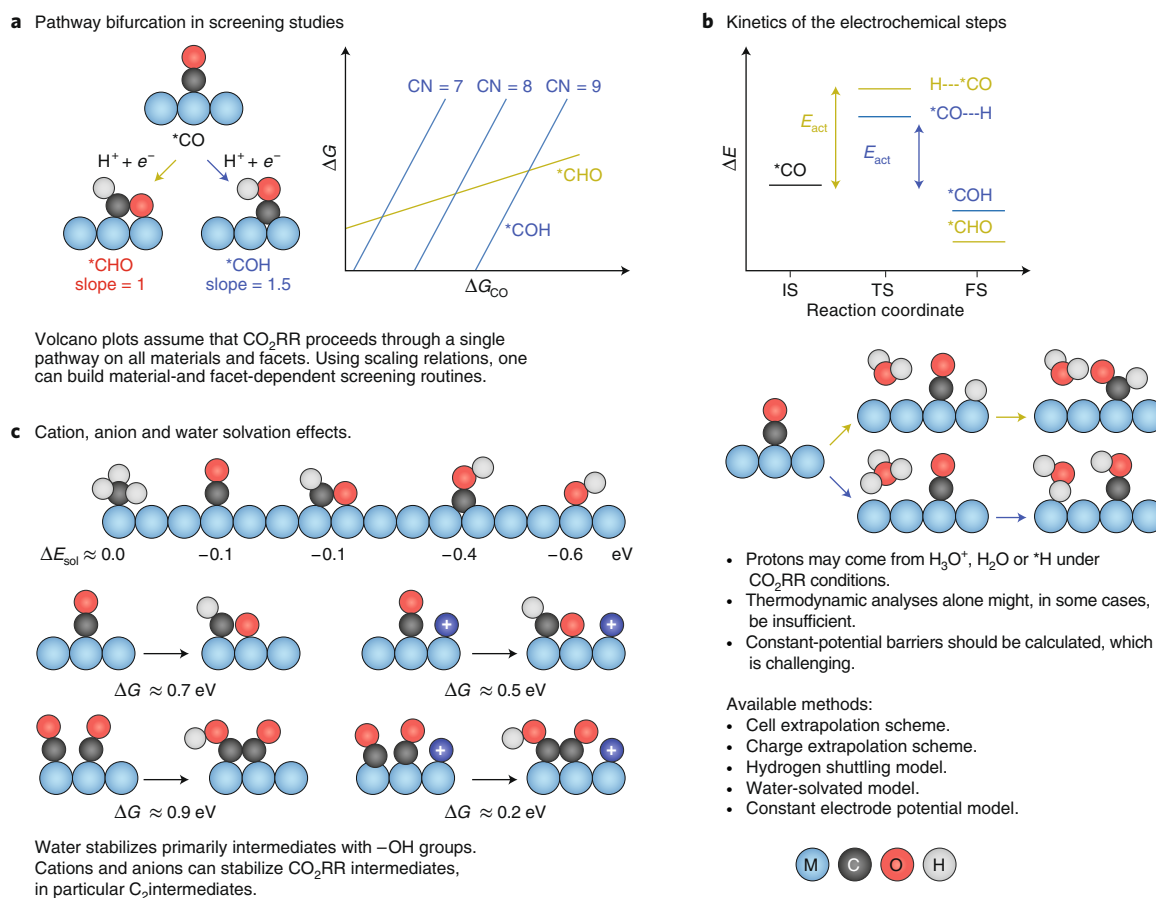
CHE-based models do not generally incorporate reaction barriers, which is another important topic under study in CO_2 and CO electroreduction models (Fig. 6b)[162–164]. An elementary-step kinetics study on the CO₂RR mechanism to C_1 products showed the formation of either *CHO or *COH from *CO hydrogenation, which determines the selectivity on Cu(111)[43] . *CH$_x$ species are formed via the more kinetically favourable *COH intermediate, which eventually leads to methane and ethylene. Cell[164] and charge[162,163] extrapolation schemes, and constant electrode potential models[44] are also available for the evaluation of energy landscapes, and recent studies have shed light on the intricacies of those methods and the important role of solvation on them[165].

Recently, it was argued[166] that adsorbate solvation had not been (sufficiently) taken into account in previous studies[40,43], and a mechanism on Cu(111) was proposed in which surface water influences the selectivity towards hydrocarbons compared with alcohol products. Although solvation is crucial when attempts are made to break scaling relations, it is often overlooked or taken into account as a constant correction to the adsorption energies calculated in vacuum

(Fig. 6c)[39,142,144,145]. It was recently found that solvation restores the scalability broken under vacuum[154] and that it strongly depends on the geometry and chemical nature of the surface sites[167–169].

Apart from the effects discussed so far, the electrolyte has been shown to alter the activity and selectivity of metal electrodes (Fig. 6c). There are two ways of incorporating ion effects in DFT simulations: implicitly and explicitly. Implicit ion effects are accounted for by means of an electric field that modifies the adsorption energies[170]. In explicit calculations, the ions are introduced and relaxed in the calculations, together with the adsorbates[82,171]. Both approaches show that CO₂RR intermediates such as $*CO_2$, *CO, *OCCO and *COCOH are stabilized by alkaline cations, and that this stabilization is related to their polar/charged character[30,80].

In short, significant progress has been made in the past decade yet numerous challenges still lie ahead, which currently prevent the development of accurate screening routines for the design of new CO_2 and CO reduction materials[172]. While we need comprehensive fundamental studies that incorporate more features of real interfaces at which CO₂RR takes place, we also need to make less problematic assumptions in screening studies aimed at designing novel materials. To date, reports of in silico-designed catalysts for

a Pathway bifurcation in screening studies

*CO

H$^+$ + e$^-$ H$^+$ + e$^-$

*CHO
slope = 1

*COH
slope = 1.5

CN = 7   CN = 8   CN = 9

ΔG

*CHO

*COH

ΔG_{CO}

Volcano plots assume that CO$_2$RR proceeds through a single pathway on all materials and facets. Using scaling relations, one can build material-and facet-dependent screening routines.

b Kinetics of the electrochemical steps

H---*CO
*CO---H

ΔE

E_{act} E_{act}

*CO

*COH
*CHO

IS   TS   FS
Reaction coordinate

• Protons may come from H$_3$O$^+$, H$_2$O or *H under CO$_2$RR conditions.
• Thermodynamic analyses alone might, in some cases, be insufficient.
• Constant-potential barriers should be calculated, which is challenging.

Available methods:
• Cell extrapolation scheme.
• Charge extrapolation scheme.
• Hydrogen shuttling model.
• Water-solvated model.
• Constant electrode potential model.

c Cation, anion and water solvation effects.

$\Delta E_{sol} \approx 0.0$ −0.1   −0.1   −0.4   −0.6   eV

$\Delta G \approx 0.7$ eV $\Delta G \approx 0.5$ eV

$\Delta G \approx 0.9$ eV $\Delta G \approx 0.2$ eV

Water stabilizes primarily intermediates with −OH groups. Cations and anions can stabilize CO$_2$RR intermediates, in particular C$_2$ intermediates.

M   C   O   H

Fig. 6 | Recent progress in descriptor-based analyses. a, Material- and facet-dependent elaboration of reaction pathways for screening studies on the example of *CO hydrogenation, which leads to *CHO or *COH depending on the type of metal and its coordination. CN, coordination number of the adsorption sites. The slopes reported are those of the scaling relations versus *CO (ref. [161]). The colour code is provided as an inset. Panel adapted from ref. [161], American Chemical Society. **b**, Kinetics of the electrochemical steps, which can be assessed using different approaches[43,44,162-165]. IS, TS and FS are the initial, transition and final states, respectively. The example shown considers *CO hydrogenation on Cu(111): while *CHO is more stable, the barrier to produce *COH is lower[43]. **c**, Effects of water solvation and ionic species on the relative stability of CO$_2$RR intermediates. Adsorbates are differently stabilized by water depending on their chemical structure. CO hydrogenation to *CHO is made 0.2 eV more favourable by cations, while CO dimerization and hydrogenation is made 0.7 eV more favourable by the same cations. Values taken from refs. [39,82,144,161,167].

CO$_2$/CO reduction to hydrocarbons and/or oxygenates successfully implemented experimentally are rare. Hopefully, future advances in the treatment of pH- and potential-dependent reaction barriers, inclusion of solvation and electrolyte effects, and a deeper understanding of scaling relations, how and when to break or avoid them, will enable such developments. To enhance the theory–experiment interplay, more single-crystal-based onset potentials and the detection of more CO$_2$RR intermediates would help in the validation or reformulation of DFT-based reaction pathways.

Future directions

In recent decades, significant progress has been made mainly regarding the design of highly active or selective electrocatalysts, and their CO$_2$RR mechanism. However, it is crucial to realize the importance of other aspects, such as electrode morphology, (sub)surface structure, and reaction and process conditions, not only from a mechanistic standpoint but also from a system perspective. Specifically, not only the electrode/electrolyte interface should be studied but also transport phenomena, catalyst stability and electrolyte/solvent effects should be optimized. In this endeavour, it is desirable and even necessary to combine computational and in situ spectroelectrochemical techniques. Ideally, one would like to combine all the different aspects in a (computational) model instead of a collection

of theoretical models providing only (mechanistic) information for specific cases. This would require a more rigorous standardization of experimental setups and procedures, more dedicated efforts to understand electrocatalysis beyond what happens at the catalyst surface, and a multiscale computational modelling approach encompassing all these aspects. We believe that future research should deviate from solely finding or improving highly active/selective electrocatalysts, and focus on the joint action of all relevant aspects for CO$_2$RR to become a viable option for the production of electrofuels.

References

1. Whipple, D. T. & Kenis, P. J. A. Prospects of CO$_2$ utilization via direct heterogeneous electrochemical reduction. *J. Phys. Chem. Lett.* **1**, 3451–3458 (2010).
2. Durst, J. et al. Electrochemical CO$_2$ reduction — a critical view on fundamentals, materials and applications. *Chim. Int. J. Chem.* **69**, 769–776 (2015).
3. Jones, J. P., Prakash, G. K. S. & Olah, G. A. Electrochemical CO$_2$ reduction: recent advances and current trends. *Isr. J. Chem.* **54**, 1451–1466 (2014).
4. Hori, Y. in *Modern Aspects of Electrochemistry* (eds Vayenas, C., White, R. & Gamboa-Aldeco, M.) 89–189 (Springer, 2008).

5. Bushuyev, O. S. et al. What should we make with CO_2 and how can we make it? *joule* **2**, 825–832 (2018).

6. Kortlever, R., Shen, J., Schouten, K. J. P., Calle-Vallejo, F. & Koper, M. T. M. Catalysts and reaction pathways for the electrochemical reduction of carbon dioxide. *J. Phys. Chem. Lett.* **6**, 4073–4082 (2015).

7. Seh, Z. W. et al. Combining theory and experiment in electrocatalysis: insights into materials design. *Science* **355**, eaad4998 (2017).

8. Hori, Y., Wakebe, H., Tsukamoto, T. & Koga, O. Electrocatalytic process of CO selectivity in electrochemical reduction of CO_2 at metal electrodes in aqueous media. *Electrochim. Acta* **39**, 1833–1839 (1994).

9. Kortlever, R., Peters, I., Koper, S. & Koper, M. T. M. Electrochemical CO_2 reduction to formic acid at low overpotential and with high Faradaic efficiency on carbon-supported bimetallic Pd–Pt nanoparticles. *ACS Catal.* **5**, 3916–3923 (2015).

10. Armstrong, F. A. & Hirst, J. Reversibility and efficiency in electrocatalytic energy conversion and lessons from enzymes. *Proc. Natl Acad. Sci. USA* **108**, 14049–14054 (2011).

11. Yoo, J. S., Christensen, R., Vegge, T., Nørskov, J. K. & Studt, F. Theoretical insight into the trends that guide the electrochemical reduction of carbon dioxide to formic acid. *ChemSusChem* **9**, 358–363 (2016).

12. Göttle, A. J. & Koper, M. T. M. Proton-coupled electron transfer in the electrocatalysis of CO_2 reduction: prediction of sequential vs. concerted pathways using DFT. *Chem. Sci.* **8**, 458–465 (2017).

13. Shen, J. et al. Electrocatalytic reduction of carbon dioxide to carbon monoxide and methane at an immobilized cobalt protoporphyrin. *Nat. Commun.* **6**, 8177 (2015).

14. Shen, J., Kolb, M. J., Göttle, A. J. & Koper, M. T. M. DFT study on the mechanism of the electrochemical reduction of CO_2 catalyzed by cobalt porphyrins. *J. Phys. Chem. C* **120**, 15714–15721 (2016).

15. Wuttig, A., Yaguchi, M., Motobayashi, K., Osawa, M. & Surendranath, Y. Inhibited proton transfer enhances Au-catalyzed CO_2-to-fuels selectivity. *Proc. Natl Acad. Sci. USA* **113**, E4585–E4593 (2016).

16. Chen, L. D., Urushihara, M., Chan, K. & Nørskov, J. K. Electric field effects in electrochemical CO_2 reduction. *ACS Catal.* **6**, 7133–7139 (2016).

17. Singh, M. R., Goodpaster, J. D., Weber, A. Z., Head-gordon, M. & Bell, A. T. Mechanistic insights into electrochemical reduction of CO_2 over Ag using density functional theory and transport models. *Proc. Natl Acad. Sci. USA* **114**, E8812–E8821 (2017).

18. Birdja, Y. Y., Shen, J. & Koper, M. T. M. Influence of the metal center of metalloprotoporphyrins on the electrocatalytic CO_2 reduction to formic acid. *Catal. Today* **288**, 37–47 (2017).

19. Solis, B. H., Maher, A. G., Dogutan, D. K., Nocera, D. G. & Hammes-Schiffer, S. Nickel phlorin intermediate formed by proton-coupled electron transfer in hydrogen evolution mechanism. *Proc. Natl Acad. Sci. USA* **113**, 485–492 (2016).

20. Göttle, A. J. & Koper, M. T. M. Determinant role of the electrogenerated reactive nucleophilic species on the selectivity during the reduction of CO_2 catalyzed by metalloporphyrins. *J. Am. Chem. Soc.* **140**, 4826–4834 (2018).

21. Loewen, N. D., Neelakantan, T. V. & Berben, L. A. Renewable formate from C–H bond formation with CO_2: using iron carbonyl clusters as electrocatalysts. *Acc. Chem. Res.* **50**, 2362–2370 (2017).

22. Tang, Q. et al. Lattice-hydride mechanism in electrocatalytic CO_2 reduction by structurally precise copper-hydride nanoclusters. *J. Am. Chem. Soc.* **139**, 9728–9736 (2017).

23. Min, X. & Kanan, M. W. Pd-catalyzed electrohydrogenation of carbon dioxide to formate: high mass activity at low overpotential and identification of the deactivation pathway. *J. Am. Chem. Soc.* **137**, 4701–4708 (2015).

24. Groenenboom, M. C. & Keith, J. A. Quantum chemical analyses of BH_4^- and BH_3OH^- hydride transfers to CO_2 in aqueous solution with potentials of mean force. *ChemPhysChem* **18**, 3148–3152 (2017).

25. Torelli, D. A. et al. Nickel-gallium-catalyzed electrochemical reduction of CO_2 to highly reduced products at low overpotentials. *ACS Catal.* **6**, 2100–2104 (2016).

26. Kortlever, R. et al. Palladium–gold catalyst for the electrochemical reduction of CO_2 to C_1–C_5 hydrocarbons. *Chem. Commun.* **52**, 10229–10232 (2016).

27. Calvinho, K. U. D. et al. Selective CO_2 reduction to C_3 and C_4 oxyhydrocarbons on nickel phosphides at overpotentials as low as 10 mV. *Energy Environ. Sci.* **11**, 2550–2559 (2018).

28. Fan, Q. et al. Electrochemical CO_2 reduction to C_{2+} species: heterogeneous electrocatalysts, reaction pathways, and optimization strategies. *Mater. Today Energy* **10**, 280–301 (2018).

29. Han, Z., Kortlever, R., Chen, H.-Y., Peters, J. C. & Agapie, T. CO_2 reduction selective for $C_{\geq 2}$ products on polycrystalline copper with N-substituted pyridinium additives. *ACS Cent. Sci.* **3**, 853–859 (2017).

30. Hoang, T. T. H. et al. Nano porous copper-silver alloys by additive-controlled electro-deposition for the selective electroreduction of CO_2 to ethylene and ethanol. *J. Am. Chem. Soc.* **140**, 5791–5797 (2018).

31. Dinh, C., Burdyny, T., Kibria, G., Seifitokaldani, A. & Christine, M. CO_2 electroreduction to ethylene via hydroxide-mediated copper catalysis at an abrupt interface. *Science* **360**, 783–787 (2018).

32. Gao, D. et al. Activity and selectivity control in CO_2 electroreduction to multicarbon products over CuO_x catalysts via electrolyte design. *ACS Catal.* **8**, 10012–10020 (2018).

33. Hori, Y., Takahashi, I., Koga, O. & Hoshi, N. Electrochemical reduction of carbon dioxide at various series of copper single crystal electrodes. *J. Mol. Catal. A* **199**, 39–47 (2003).

34. Schouten, K. J. P., Kwon, Y., van der Ham, C. J. M., Qin, Z. & Koper, M. T. M. A new mechanism for the selectivity to C_1 and C_2 species in the electrochemical reduction of carbon dioxide on copper electrodes. *Chem. Sci.* **2**, 1902–1909 (2011).

35. Schouten, K., Gallent, E. & Koper, M. Structure sensitivity of the electrochemical reduction of carbon monoxide on copper single crystals. *ACS Catal.* **4**, 1292–1295 (2013).

36. Schouten, K. J. P., Qin, Z., Gallent, E. P. & Koper, M. T. M. Two pathways for the formation of ethylene in CO reduction on single-crystal copper electrodes. *J. Am. Chem. Soc.* **134**, 9864–9867 (2012).

37. Gattrell, M., Gupta, N. & Co, A. A review of the aqueous electrochemical reduction of CO_2 to hydrocarbons at copper. *J. Electroanal. Chem.* **594**, 1–19 (2006).

38. Wuttig, A. et al. Tracking a common surface-bound intermediate during CO_2-to-fuels catalysis. *ACS Cent. Sci.* **2**, 522–528 (2016).

39. Calle-Vallejo, F. & Koper, M. T. M. Theoretical considerations on the electroreduction of CO to C_2 species on Cu(100) electrodes. *Angew. Chem. Int. Ed.* **52**, 7282–7285 (2013).

40. Montoya, J. H., Shi, C., Chan, K. & Nørskov, J. K. Theoretical insights into a CO dimerization mechanism in CO_2 electroreduction. *J. Phys. Chem. Lett.* **6**, 2032–2037 (2015).

41. Goodpaster, J. D., Bell, A. T. & Head-Gordon, M. Identification of possible pathways for C–C bond formation during electrochemical reduction of CO_2: new theoretical insights from an improved electrochemical model. *J. Phys. Chem. Lett.* **7**, 1471–1477 (2016).

42. Li, H., Li, Y., Koper, M. T. M. & Calle-Vallejo, F. Bond making and breaking between carbon, nitrogen and oxygen in electrocatalysis. *J. Am. Chem. Soc.* **136**, 15694–15701 (2014).

43. Nie, X., Esopi, M. R., Janik, M. J. & Asthagiri, A. Selectivity of CO_2 reduction on copper electrodes: the role of the kinetics of elementary steps. *Angew. Chem. Int. Ed.* **52**, 2459–2462 (2013).

44. Garza, A., Bell, A. T. & Head-Gordon, M. Mechanism of CO_2 reduction at copper surfaces: pathways to C_2 products. *ACS Catal.* **8**, 1490–1499 (2018).

45. Pérez-Gallent, E., Figueiredo, M. C., Calle-Vallejo, F. & Koper, M. T. M. Spectroscopic observation of a hydrogenated CO dimer intermediate during CO reduction on Cu(100) electrodes. *Angew. Chem. Int. Ed.* **56**, 3621–3624 (2017).

46. Kas, R., Kortlever, R., Yilmaz, H., Koper, M. T. M. & Mul, G. Manipulating the hydrocarbon selectivity of copper nanoparticles in CO_2 electroreduction by process conditions. *ChemElectroChem* **2**, 354–358 (2015).

47. Hanselman, S., Koper, M. T. M. & Calle-Vallejo, F. Computational comparison of late transition metal (100) surfaces for the electrocatalytic reduction of CO to C_2 species. *ACS Energy Lett.* **3**, 1062–1067 (2018).

48. Ledezma-Yanez, I., Gallent, E. P., Koper, M. T. M. & Calle-Vallejo, F. Structure-sensitive electroreduction of acetaldehyde to ethanol on copper and its mechanistic implications for CO and CO_2 reduction. *Catal. Today* **262**, 90–94 (2016).

49. Hahn, C. et al. Engineering Cu surfaces for the electrocatalytic conversion of CO_2: controlling selectivity toward oxygenates and hydrocarbons. *Proc. Natl Acad. Sci. USA* **114**, 5918–5923 (2017).

50. Ren, D., Ang, B. S.-H. & Yeo, B. S. Tuning the selectivity of carbon dioxide electroreduction toward ethanol on oxide-derived Cu_xZn catalysts. *ACS Catal.* **6**, 8239–8247 (2016).

51. Liu, Y., Chen, S., Quan, X. & Yu, H. Efficient electrochemical reduction of carbon dioxide to acetate on nitrogen-doped nanodiamond. *J. Am. Chem. Soc.* **137**, 11631–11636 (2015).

52. Genovese, C., Ampelli, C., Perathoner, S. & Centi, G. Mechanism of C–C bond formation in the electrocatalytic reduction of CO_2 to acetic acid. A challenging reaction to use renewable energy with chemistry. *Green. Chem.* **19**, 2406–2415 (2017).

53. Birdja, Y. Y. & Koper, M. T. M. The importance of Cannizzaro-type reactions during electrocatalytic reduction of carbon dioxide. *J. Am. Chem. Soc.* **139**, 2030–2034 (2017).

54. Zhuang, T. T. et al. Copper nanocavities confine intermediates for efficient electrosynthesis of C3 alcohol fuels from carbon monoxide. *Nat. Catal.* **1**, 946–951 (2018).

55. Kuhl, K. P., Cave, E. R., Abram, D. N. & Jaramillo, T. F. New insights into the electrochemical reduction of carbon dioxide on metallic copper surfaces. *Energy Environ. Sci.* **5**, 7050–7059 (2012).

56. Ren, D., Wong, N. T., Handoko, A. D., Huang, Y. & Yeo, B. S. Mechanistic insights into the enhanced activity and stability of agglomerated Cu nanocrystals for the electrochemical reduction of carbon dioxide to *n*-propanol. *J. Phys. Chem. Lett.* **7**, 20–24 (2016).

57. Singh, M. R. et al. Effects of electrolyte, catalyst, and membrane composition and operating conditions on the performance of solar-driven electrochemical reduction of carbon dioxide. *Phys. Chem. Chem. Phys.* **17**, 18924–18936 (2015).

58. Clark, E. L. et al. Standards and protocols for data acquisition and reporting for studies of the electrochemical reduction of carbon dioxide. *ACS Catal.* **8**, 6560–6570 (2018).

59. Zhong, H., Fujii, K., Nakano, Y. & Jin, F. Effect of CO_2 bubbling into aqueous solutions used for electrochemical reduction of CO_2 for energy conversion and storage. *J. Phys. Chem. C.* **119**, 55–61 (2015).

60. Sreekanth, N. & Phani, K. L. Selective reduction of CO_2 to formate through bicarbonate reduction on metal electrodes: new insights gained from SG/TC mode of SECM. *Chem. Commun.* **50**, 11143–11146 (2014).

61. Kortlever, R., Tan, K. H., Kwon, Y. & Koper, M. T. M. Electrochemical carbon dioxide and bicarbonate reduction on copper in weakly alkaline media. *J. Solid State Electrochem.* **17**, 1843–1849 (2013).

62. Innocent, B. et al. FTIR spectroscopy study of the reduction of carbon dioxide on lead electrode in aqueous medium. *Appl. Catal. B* **94**, 219–224 (2010).

63. Dunwell, M. et al. The central role of bicarbonate in the electrochemical reduction of carbon dioxide on gold. *J. Am. Chem. Soc.* **139**, 3774–3783 (2017).

64. Zhu, S., Jiang, B., Cai, W. Bin & Shao, M. Direct observation on reaction intermediates and the role of bicarbonate anions in CO_2 electrochemical reduction reaction on Cu surfaces. *J. Am. Chem. Soc.* **139**, 15664–15667 (2017).

65. Wuttig, A., Yoon, Y., Ryu, J. & Surendranath, Y. Bicarbonate is not a general acid in Au-catalyzed CO_2 electroreduction. *J. Am. Chem. Soc.* **139**, 17109–17113 (2017).

66. Resasco, J., Lum, Y., Clark, E., Zeledon, J. Z. & Bell, A. T. Effects of anion identity and concentration on electrochemical reduction of CO_2. *ChemElectroChem* **5**, 1064–1072 (2018).

67. Varela, A. S., Kroschel, M., Reier, T. & Strasser, P. Controlling the selectivity of CO_2 electroreduction on copper: the effect of the electrolyte concentration and the importance of the local pH. *Catal. Today* **260**, 8–13 (2016).

68. Dunwell, M. et al. Examination of near-electrode concentration gradients and kinetic impacts on the electrochemical reduction of CO_2 using surface-enhanced infrared spectroscopy. *ACS Catal.* **8**, 3999–4008 (2018).

69. Gupta, N., Gattrell, M. & MacDougall, B. Calculation for the cathode surface concentrations in the electrochemical reduction of CO_2 in $KHCO_3$ solutions. *J. Appl. Electrochem.* **36**, 161–172 (2006).

70. Hashiba, H. et al. Effects of electrolyte buffer capacity on surface reactant species and reaction rate of CO_2 in electrochemical CO_2 reduction. *J. Phys. Chem. C.* **122**, 3719–3726 (2018).

71. Liu, X. et al. pH effects on the electrochemical reduction of $CO_{(2)}$ towards C_2 products on stepped copper. *Nat. Commun.* **10**, 32 (2019).

72. Hori, Y., Murata, A. & Takahashi, R. Formation of hydrocarbons in the electrochemical reduction of carbon dioxide at a copper electrode in aqueous solution. *J. Chem. Soc. Faraday Trans. 1* **85**, 2309–2326 (1989).

73. Yoon, Y., Hall, A. S. & Surendranath, Y. Tuning of silver catalyst mesostructure promotes selective carbon dioxide conversion into fuels. *Angew. Chem. Int. Ed.* **55**, 15282–15286 (2016).

74. Hall, A. S., Yoon, Y., Wuttig, A. & Surendranath, Y. Mesostructure-induced selectivity in CO_2 reduction catalysis. *J. Am. Chem. Soc.* **137**, 14834–14837 (2015).

75. Lim, C. F. C., Harrington, D. A. & Marshall, A. T. Effects of mass transfer on the electrocatalytic CO_2 reduction on Cu. *Electrochim. Acta* **238**, 56–63 (2017).

76. Ooka, H., Figueiredo, M. C. & Koper, M. T. M. Competition between hydrogen evolution and carbon dioxide reduction on copper electrodes in mildly acidic media. *Langmuir* **33**, 9307–9313 (2017).

77. Luca, O. R. & Fenwick, A. Q. Organic reactions for the electrochemical and photochemical production of CO_2 to fuels — the reduction chemistry of carboxylic acids as bent CO_2 surrogates, aldehydes, alcohols and alkyls. *J. Photochem. Photobiol. B* **152**, 26–42 (2015).

78. Murata, A. & Hori, Y. Product selectivity affected by cationic species in electrochemical reduction of CO_2 and CO at a Cu electrode. *Bull. Chem. Soc. Jpn* **64**, 123–127 (1991).

79. Singh, M. R., Kwon, Y., Lum, Y., Ager, J. W. & Bell, A. T. Hydrolysis of electrolyte cations enhances the electrochemical reduction of CO_2 over Ag and Cu. *J. Am. Chem. Soc.* **138**, 13006–13012 (2016).

80. Thorson, M. R., Siil, K. I. & Kenis, P. J. A. Effect of cations on the electrochemical conversion of CO_2 to CO. *J. Electrochem. Soc.* **160**, F69–F74 (2013).

81. Resasco, J. et al. Promoter effects of alkali metal cations on the electrochemical reduction of carbon dioxide. *J. Am. Chem. Soc.* **139**, 11277–11287 (2017).

82. Pérez-Gallent, E., Marcandalli, G., Figueiredo, M. C., Calle-Vallejo, F. & Koper, M. T. M. Structure- and potential-dependent cation effects on CO reduction at copper single-crystal electrodes. *J. Am. Chem. Soc.* **139**, 16412–16419 (2017).

83. Yano, H., Tanaka, T., Nakayama, M. & Ogura, K. Selective electrochemical reduction of CO_2 to ethylene at a three-phase interface on copper(I) halide-confined Cu-mesh electrodes in acidic solutions of potassium halides. *J. Electroanal. Chem.* **565**, 287–293 (2004).

84. Ogura, K., Ferrell, J. R., Cugini, A. V., Smotkin, E. S. & Salazar-Villalpando, M. D. CO_2 attraction by specifically adsorbed anions and subsequent accelerated electrochemical reduction. *Electrochim. Acta* **56**, 381–386 (2010).

85. Varela, A. S., Ju, W., Reier, T. & Strasser, P. Tuning the catalytic activity and selectivity of Cu for CO_2 electroreduction in the presence of halides. *ACS Catal.* **6**, 2136–2144 (2016).

86. Gao, D., Scholten, F. & Roldan Cuenya, B. Improved CO_2 electroreduction performance on plasma-activated Cu catalysts via electrolyte design: halide effect. *ACS Catal.* **7**, 5112–5120 (2017).

87. Huang, Y., Ong, C. W. & Yeo, B. S. Effects of electrolyte anions on the reduction of carbon dioxide to ethylene and ethanol on copper (100) and (111) surfaces. *ChemSusChem* **11**, 3299–3306 (2018).

88. Tang, W. et al. The importance of surface morphology in controlling the selectivity of polycrystalline copper for CO_2 electroreduction. *Phys. Chem. Chem. Phys.* **14**, 76–81 (2012).

89. Roberts, F. S., Kuhl, K. P. & Nilsson, A. High selectivity for ethylene from carbon dioxide reduction over copper nanocube electrocatalysts. *Angew. Chem. Int. Ed.* **54**, 5179–5182 (2015).

90. Loiudice, A. et al. Tailoring copper nanocrystals towards C_2 products in electrochemical CO_2 reduction. *Angew. Chem. Int. Ed.* **55**, 5789–5792 (2016).

91. Sen, S., Liu, D. & Palmore, G. T. R. Electrochemical reduction of CO_2 at copper nanofoams. *ACS Catal.* **4**, 3091–3095 (2014).

92. Reske, R., Mistry, H., Behafarid, F., Roldan Cuenya, B. & Strasser, P. Particle size effects in the catalytic electroreduction of CO_2 on Cu nanoparticles. *J. Am. Chem. Soc.* **136**, 6978–6986 (2014).

93. Yang, K. D. et al. Morphology-directed selective production of ethylene or ethane from CO_2 on a Cu mesopore electrode. *Angew. Chem. Int. Ed.* **56**, 796–800 (2017).

94. Chen, C. S. et al. Stable and selective electrochemical reduction of carbon dioxide to ethylene on copper mesocrystals. *Catal. Sci. Technol.* **5**, 161–168 (2015).

95. Mistry, H. et al. Tuning catalytic selectivity at the mesoscale via interparticle interactions. *ACS Catal.* **6**, 1075–1080 (2016).

96. Kas, R. et al. Three-dimensional porous hollow fibre copper electrodes for efficient and high-rate electrochemical carbon dioxide reduction. *Nat. Commun.* **7**, 10748 (2016).

97. Li, C. W. & Kanan, M. W. CO_2 reduction at low overpotential on Cu electrodes resulting from the reduction of thick Cu_2O films. *J. Am. Chem. Soc.* **134**, 7231–7234 (2012).

98. Lee, C. H. & Kanan, M. W. Controlling H^+ vs CO_2 reduction selectivity on Pb electrodes. *ACS Catal.* **5**, 465–469 (2015).

99. Dutta, A., Rahaman, M., Luedi, N. C., Mohos, M. & Broekmann, P. Morphology matters: tuning the product distribution of CO_2 electroreduction on oxide-derived Cu foam catalysts. *ACS Catal.* **6**, 3804–3814 (2016).

100. Ma, M., Djanashvili, K. & Smith, W. A. Selective electrochemical reduction of CO_2 to CO on CuO-derived Cu nanowires. *Phys. Chem. Chem. Phys.* **17**, 20861–20867 (2015).

101. Kas, R. et al. Electrochemical CO_2 reduction on Cu_2O-derived copper nanoparticles: controlling the catalytic selectivity of hydrocarbons. *Phys. Chem. Chem. Phys.* **16**, 12194–201 (2014).

102. Li, C. W., Ciston, J. & Kanan, M. W. Electroreduction of carbon monoxide to liquid fuel on oxide-derived nanocrystalline copper. *Nature* **508**, 504–507 (2014).

103. Chen, Y., Li, C. W. & Kanan, M. W. Aqueous CO_2 reduction at very low overpotential on oxide-derived Au nanoparticles. *J. Am. Chem. Soc.* **134**, 19969–19972 (2012).

104. Ma, M., Trześniewski, B. J., Xie, J. & Smith, W. A. Selective and efficient reduction of carbon dioxide to carbon monoxide on oxide-derived nanostructured silver electrocatalysts. *Angew. Chem. Int. Ed.* **55**, 9748–9752 (2016).

105. Pander, J. E. et al. Understanding the heterogeneous electrocatalytic reduction of carbon dioxide on oxide-derived catalysts. *ChemElectroChem* **5**, 219–237 (2018).

106. Zhu, W. et al. Monodisperse Au nanoparticles for selective electrocatalytic reduction of CO_2 to CO. *J. Am. Chem. Soc.* **135**, 16833–16836 (2013).

107. Mistry, H. et al. Exceptional size-dependent activity enhancement in the electroreduction of CO_2 over Au nanoparticles. *J. Am. Chem. Soc.* **136**, 16473–16476 (2014).

108. Feng, X., Jiang, K., Fan, S. & Kanan, M. W. A direct grain-boundary-activity correlation for CO electroreduction on Cu nanoparticles. *ACS Cent. Sci.* **2**, 169–174 (2016).

109. Verdaguer-Casadevall, A. et al. Probing the active surface sites for CO reduction on oxide-derived copper electrocatalysts. *J. Am. Chem. Soc.* **137**, 9808–9811 (2015).

110. Eilert, A. et al. Subsurface Oxygen in oxide-derived copper electrocatalysts for carbon dioxide reduction. *J. Phys. Chem. Lett.* **8**, 285–290 (2017).

111. Mariano, R. G., McKelvey, K., White, H. S. & Kanan, M. W. Selective increase in CO_2 electroreduction activity at grain-boundary surface terminations. *Science* **358**, 1187–1192 (2017).

112. Mistry, H. et al. Highly selective plasma-activated copper catalysts for carbon dioxide reduction to ethylene. *Nat. Commun.* **7**, 12123 (2016).

113. Mistry, H. et al. Enhanced carbon dioxide electroreduction to carbon monoxide over defect-rich plasma-activated silver catalysts. *Angew. Chem. Int. Ed.* **56**, 11394–11398 (2017).

114. Favaro, M. et al. Subsurface oxide plays a critical role in CO_2 activation by Cu(111) surfaces to form chemisorbed CO_2, the first step in reduction of CO_2. *Proc. Natl Acad. Sci. USA* **114**, 6706–6711 (2017).

115. Xiao, J., Kuc, A., Frauenheim, T. & Heine, T. CO_2 reduction at low overpotential on Cu electrodes in the presence of impurities at the subsurface. *J. Mater. Chem. A* **2**, 4885–4889 (2014).

116. Fields, M., Hong, X., Norskov, J. K. & Chan, K. The role of subsurface oxygen on Cu surfaces for CO_2 electrochemical reduction. *J. Phys. Chem. C.* **122**, 16209–16215 (2018).

117. Lum, Y. & Ager, J. W. Stability of residual oxides in oxide-derived copper catalysts for electrochemical CO_2 reduction investigated with ^{18}O labeling. *Angew. Chem. Int. Ed.* **57**, 551–554 (2018).

118. Garza, A. J., Bell, A. T. & Head-Gordon, M. Is subsurface oxygen necessary for the electrochemical reduction of CO_2 on copper. *J. Phys. Chem. Lett.* **9**, 601–606 (2018).

119. Jiang, K. et al. Metal ion cycling of Cu foil for selective C–C coupling in electrochemical CO_2 reduction. *Nat. Catal.* **1**, 111–119 (2018).

120. Cheng, T., Xiao, H. & Goddard, W. A. Nature of the active sites for CO reduction on copper nanoparticles; suggestions for optimizing performance. *J. Am. Chem. Soc.* **139**, 11642–11645 (2017).

121. Le, M. et al. Electrochemical reduction of CO_2 to CH_3OH at copper oxide surfaces. *J. Electrochem. Soc.* **158**, E45–E49 (2011).

122. Frese, K. W. Electrochemical reduction of CO_2 at intentionally oxidized copper electrodes. *J. Electrochem. Soc.* **138**, 3338–3344 (1991).

123. Ren, D. et al. Selective electrochemical reduction of carbon dioxide to ethylene and ethanol on copper(I) oxide catalysts. *ACS Catal.* **5**, 2814–2821 (2015).

124. Chi, D. et al. Morphology-controlled CuO nanoparticles for electroreduction of CO_2 to ethanol. *RSC Adv* **4**, 37329–37332 (2014).

125. Kim, D. et al. Insights into an autonomously formed oxygen-evacuated Cu_2O electrode for the selective production of C_2H_4 from CO_2. *Phys. Chem. Chem. Phys.* **17**, 824–830 (2015).

126. Lee, S., Kim, D. & Lee, J. Electrocatalytic production of C3–C4 compounds by conversion of CO_2 on a chloride-induced bi-phasic Cu_2O–Cu catalyst. *Angew. Chem. Int. Ed.* **54**, 14701–14705 (2015).

127. Le Duff, C. S., Lawrence, M. J. & Rodriguez, P. Role of the adsorbed oxygen species in the selective electrochemical reduction of CO_2 to alcohols and carbonyls on copper electrodes. *Angew. Chem. Int. Ed.* **56**, 12919–12924 (2017).

128. Ren, D., Fong, J. & Yeo, B. S. The effects of currents and potentials on the selectivities of copper toward carbon dioxide electroreduction. *Nat. Commun.* **9**, 925 (2018).

129. Trasatti, S. & Petrii, O. A. Real surface area measurement in electrochemistry. *Pure Appl. Chem.* **63**, 711–734 (1991).

130. McCrory, C. C. L., Jung, S., Peters, J. C. & Jaramillo, T. F. Benchmarking heterogeneous electrocatalysts for the oxygen evolution reaction. *J. Am. Chem. Soc.* **135**, 16977–16987 (2013).

131. Heyes, J., Dunwell, M. & Xu, B. CO_2 reduction on Cu at low overpotentials with surface-enhanced in situ spectroscopy. *J. Phys. Chem. C.* **120**, 17334–17341 (2016).

132. Gunathunge, C. M. et al. Spectroscopic observation of reversible surface reconstruction of copper electrodes under CO_2 reduction. *J. Phys. Chem. C.* **121**, 12337–12344 (2017).

133. Pander, J. E., Baruch, M. F. & Bocarsly, A. B. Probing the mechanism of aqueous CO_2 reduction on post-transition-metal electrodes using ATR-IR spectroelectrochemistry. *ACS Catal.* **6**, 7824–7833 (2016).

134. Cheng, T., Fortunelli, A. & Goddard, W. A. Reaction intermediates during operando electrocatalysis identified from full solvent quantum mechanics molecular dynamics. *Proc. Natl Acad. Sci. USA* **116**, 7718–7722 (2019).

135. Ayemoba, O. & Cuesta, A. Spectroscopic evidence of size-dependent buffering of interfacial pH by cation hydrolysis during CO_2 electroreduction. *ACS Appl. Mater. Interfaces* **9**, 27377–27382 (2017).

136. Figueiredo, M. C., Ledezma-Yanez, I. & Koper, M. T. M. In situ spectroscopic study of CO_2 electroreduction at copper electrodes in acetonitrile. *ACS Catal.* **6**, 2382–2392 (2016).

137. Eilert, A., Roberts, F. S., Friebel, D. & Nilsson, A. Formation of copper catalysts for CO_2 reduction with high ethylene/methane product ratio investigated with in situ x-ray absorption spectroscopy. *J. Phys. Chem. Lett.* **7**, 1466–1470 (2016).

138. Choi, Y. W., Mistry, H. & Roldan Cuenya, B. New insights into working nanostructured electrocatalysts through operando spectroscopy and microscopy. *Curr. Opin. Electrochem.* **1**, 95–103 (2017).

139. Handoko, A. D., Wei, F., Jenndy, Yeo, B. S. & Seh, Z. W. Understanding heterogeneous electrocatalytic carbon dioxide reduction through operando techniques. *Nat. Catal.* **1**, 922–934 (2018).

140. Zhu, S., Li, T., Cai, W.-B. & Shao, M. CO_2 electrochemical reduction as probed through infrared spectroscopy. *ACS Energy Lett.* **4**, 682–689 (2019).

141. Rendón-Calle, A., Builes, S. & Calle-Vallejo, F. A brief review of the computational modeling of CO_2 electroreduction on Cu electrodes. *Curr. Opin. Electrochem.* **9**, 158–165 (2018).

142. Nørskov, J. K. et al. Origin of the overpotential for oxygen reduction at a fuel-cell cathode. *J. Phys. Chem. B* **108**, 17886–17892 (2004).

143. Hansen, H. A., Rossmeisl, J. & Nørskov, J. K. Surface Pourbaix diagrams and oxygen reduction activity of Pt, Ag and Ni(111) surfaces studied by DFT. *Phys. Chem. Chem. Phys.* **10**, 3722–3730 (2008).

144. Peterson, A. A. et al. How copper catalyzes the electroreduction of carbon dioxide into hydrocarbon fuels. *Energy Environ. Sci.* **3**, 1311–1315 (2010).

145. Peterson, A. & Nørskov, J. Activity descriptors for CO_2 electroreduction to methane on transition metal catalysts. *J. Phys. Chem. Lett.* **3**, 251–258 (2012).

146. Saravanan, K., Basdogan, Y., Dean, J. & Keith, J. A. Computational investigation of CO_2 electroreduction on tin oxide and predictions of Ti, V, Nb and Zr dopants for improved catalysis. *J. Mater. Chem. A* **5**, 11756–11763 (2017).

147. Saravanan, K., Gottlieb, E. & Keith, J. A. Nitrogen-doped nanocarbon materials under electroreduction operating conditions and implications for electrocatalysis of CO_2. *Carbon* **111**, 859–866 (2017).

148. Koper, M. T. M. Theory of the transition from sequential to concerted electrochemical proton–electron transfer. *Phys. Chem. Chem. Phys.* **15**, 1399–1407 (2013).

149. Koper, M. T. M. Activity volcanoes for the electrocatalysis of homolytic and heterolytic hydrogen evolution. *J. Solid State Electrochem.* **20**, 895–899 (2016).

150. Abild-Pedersen, F. et al. Scaling properties of adsorption energies for hydrogen-containing molecules on transition-metal surfaces. *Phys. Rev. Lett.* **99**, 4–7 (2007).

151. Montemore, M. M. & Medlin, J. W. Scaling relations between adsorption energies for computational screening and design of catalysts. *Catal. Sci. Technol.* **4**, 3748–3761 (2014).

152. Greeley, J. Theoretical heterogeneous catalysis: scaling relationships and computational catalyst design. *Annu. Rev. Chem. Biomol. Eng.* **7**, 605–635 (2016).

153. Govindarajan, N., García-Lastra, J. M., Meijer, E. J. & Calle-Vallejo, F. Does the breaking of adsorption-energy scaling relations guarantee enhanced electrocatalysis? *Curr. Opin. Electrochem.* **8**, 110–117 (2018).

154. Calle-Vallejo, F., Krabbe, A. & Garcia-Lastra, J. M. How covalence breaks adsorption-energy scaling relations and solvation restores them. *Chem. Sci.* **8**, 124–130 (2017).

155. Shin, H., Ha, Y. & Kim, H. 2D covalent metals: a new materials domain of electrochemical CO_2 conversion with broken scaling relationship. *J. Phys. Chem. Lett.* **7**, 4124–4129 (2016).

156. Hansen, H. A., Varley, J. B., Peterson, A. A. & Norskov, J. K. Understanding trends in the electrocatalytic activity of metals and enzymes for CO_2 reduction to CO. *J. Phys. Chem. Lett.* **4**, 388–392 (2013).

157. Li, Y. & Sun, Q. Recent advances in breaking scaling relations for effective electrochemical conversion of CO_2. *Adv. Energy Mater.* **6**, 1–19 (2016).

158. Akhade, S. A., Luo, W., Nie, X., Asthagiri, A. & Janik, M. J. Theoretical insight on reactivity trends in CO_2 electroreduction across transition metals. *Catal. Sci. Technol.* **6**, 1042–1053 (2016).

159. Cheng, M. J., Kwon, Y., Head-Gordon, M. & Bell, A. T. Tailoring metal-porphyrin-like active sites on graphene to improve the efficiency and selectivity of electrochemical CO_2 reduction. *J. Phys. Chem. C.* **119**, 21345–21352 (2015).

160. Khorshidi, A., Violet, J., Hashemi, J. & Peterson, A. A. How strain can break the scaling relations of catalysis. *Nat. Catal.* **1**, 263–268 (2018).

161. Calle-Vallejo, F. & Koper, M. T. M. Accounting for bifurcating pathways in the screening for CO_2 reduction catalysts. *ACS Catal.* **7**, 7346–7351 (2017).

162. Shi, C., Chan, K., Yoo, J. S. & Nørskov, J. K. Barriers of electrochemical CO_2 reduction on transition metals. *Org. Process Res. Dev.* **20**, 1424–1430 (2016).

163. Chan, K. & Nørskov, J. K. Electrochemical barriers made simple. *J. Phys. Chem. Lett.* **6**, 2663–2668 (2015).

164. Hussain, J., Jónsson, H. & Skúlason, E. Calculations of product selectivity in electrochemical CO_2 reduction calculations of product selectivity in electrochemical CO_2 reduction. *ACS Catal.* **8**, 5240–5249 (2018).

165. Gauthier, J. A. et al. Challenges in modeling electrochemical reaction energetics with polarizable continuum models. *ACS Catal.* **9**, 920–931 (2019).

166. Xiao, H., Cheng, T. & Goddard, W. A. Atomistic mechanisms underlying selectivities in C_1 and C_2 products from electrochemical reduction of CO on Cu(111). *J. Am. Chem. Soc.* **139**, 130–136 (2017).

167. He, Z.-D., Hanselman, S., Chen, Y. X., Koper, M. T. M. & Calle-Vallejo, F. Importance of solvation for the accurate prediction of oxygen reduction activities of Pt-based electrocatalysts. *J. Phys. Chem. Lett.* **8**, 2243–2246 (2017).

168. Tripkovic, V. Thermodynamic assessment of the oxygen reduction activity in aqueous solutions. *Phys. Chem. Chem. Phys.* **19**, 29381–29388 (2017).

169. Ludwig, T. et al. Solvent–adsorbate interactions and adsorbate-specific solvent structure in carbon dioxide reduction on a stepped Cu surface. *J. Phys. Chem. C.* **123**, 5999–6009 (2019).

170. Resasco, J. et al. Promoter effects of alkali metal cations on the electrochemical reduction of carbon dioxide. *J. Am. Chem. Soc.* **139**, 11277–11287 (2017).

171. Akhade, S. A., McCrum, I. T. & Janik, M. J. The impact of specifically adsorbed ions on the copper-catalyzed electroreduction of CO_2. *J. Electrochem. Soc.* **163**, F477–F484 (2016).

172. Jovanov, Z. P. et al. Opportunities and challenges in the electrocatalysis of CO_2 and CO reduction using bifunctional surfaces: a theoretical and experimental study of Au–Cd alloys. *J. Catal.* **343**, 215–231 (2016).

173. Cave, E. R. et al. Electrochemical CO_2 reduction on Au surfaces: mechanistic aspects regarding the formation of major and minor products. *Phys. Chem. Chem. Phys.* **19**, 15856–15863 (2017).

174. Hatsukade, T., Kuhl, K. P., Cave, E. R., Abram, D. N. & Jaramillo, T. F. Insights into the electrocatalytic reduction of CO_2 on metallic silver surfaces. *Phys. Chem. Chem. Phys.* **16**, 13814–13819 (2014).

175. Frese Jr., K. W., Leach, S. C. & Summers, D. P. Electrochemical reduction of aqueous carbon dioxide to methanol. US patent 4609441A (1986).

176. Song, Y. et al. High-selectivity electrochemical conversion of CO_2 to ethanol using a copper nanoparticle/N-doped graphene electrode. *ChemistrySelect* **1**, 6055–6061 (2016).

Competing interests

The authors declare no competing interests.

Additional information

Reprints and permissions information is available at www.nature.com/reprints.

Correspondence should be addressed to F.C.-V. or M.T.M.K.

Publisher's note: Springer Nature remains neutral with regard to jurisdictional claims in published maps and institutional affiliations.